nature medicine

ARTICLES

https://doi.org/10.1038/s41591-020-0827-2

Locoregional delivery of CAR T cells to the cerebrospinal fluid for treatment of metastatic medulloblastoma and ependymoma

Laura K. Donovan[1,2], Alberto Delaidelli[3], Sujith K. Joseph[4,5], Kevin Bielamowicz[4,5], Kristen Fousek[4,5], Borja L. Holgado[1,2], Alex Manno[1,2], Dilakshan Srikanthan[1,2,6], Ahmed Z. Gad[4,5], Randy Van Ommeren[1,2,6], David Przelicki[1,2,6], Cory Richman[1,2,7], Vijay Ramaswamy[1,8], Craig Daniels[1,2], Jonelle G. Pallota[1,2], Tajana Douglas[1,2], Alyssa C. M. Joynt[1,2], Joonas Haapasalo[1,2], Carolina Nor[1,2], Maria C. Vladoiu[1,2,6], Claudia M. Kuzan-Fischer[1,2], Livia Garzia[9], Stephen C. Mack[10], Srinidhi Varadharajan[10], Matthew L. Baker[5], Liam Hendrikse[1,2,7], Michelle Ly[1,2,6], Kaitlin Kharas[1,2,6], Polina Balin[1,2,6], Xiaochong Wu[1,2], Lei Qin[1,2], Ning Huang[1,2], Ana Guerreiro Stucklin[1,2], A. Sorana Morrissy[11,12], Florence M. G. Cavalli[1,2], Betty Luu[1,2], Raul Suarez[1,2], Pasqualino De Antonellis[1,2], Antony Michealraj[1,2], Avesta Rastan[1,2], Meenakshi Hegde[4,5], Martin Komosa[1,2], Olga Sirbu[1,2,7], Sachin A. Kumar[1,2], Zied Abdullaev[13], Claudia C. Faria[14], Stephen Yip[15], Juliette Hukin[16], Uri Tabori[1,2], Cynthia Hawkins[1,2], Ken Aldape[13], Mads Daugaard[17,18], John M. Maris[19,20,21], Poul H. Sorensen[3], Nabil Ahmed[4,5] and Michael D. Taylor[1,2,22,23] ✉

Recurrent medulloblastoma and ependymoma are universally lethal, with no approved targeted therapies and few candidates presently under clinical evaluation. Nearly all recurrent medulloblastomas and posterior fossa group A (PFA) ependymomas are located adjacent to and bathed by the cerebrospinal fluid, presenting an opportunity for locoregional therapy, bypassing the blood–brain barrier. We identify three cell-surface targets, EPHA2, HER2 and interleukin 13 receptor α2, expressed on medulloblastomas and ependymomas, but not expressed in the normal developing brain. We validate intrathecal delivery of EPHA2, HER2 and interleukin 13 receptor α2 chimeric antigen receptor T cells as an effective treatment for primary, metastatic and recurrent group 3 medulloblastoma and PFA ependymoma xenografts in mouse models. Finally, we demonstrate that administration of these chimeric antigen receptor T cells into the cerebrospinal fluid, alone or in combination with azacytidine, is a highly effective therapy for multiple metastatic mouse models of group 3 medulloblastoma and PFA ependymoma, thereby providing a rationale for clinical trials of these approaches in humans.

Brain tumors are the most predominant cause of pediatric cancer deaths[1]. Medulloblastomas are the most common malignant childhood brain tumor[2] and ependymomas are the third most common[3]; both lead to morbidity and mortality in affected patients and are essentially incurable at the time of recurrence[4,5]. Targeted therapies for medulloblastoma and ependymoma have been slow to

[1]The Arthur and Sonia Labatt Brain Tumour Research Centre, The Hospital for Sick Children, Toronto, Ontario, Canada. [2]Developmental & Stem Cell Biology Program, The Hospital for Sick Children, Toronto, Ontario, Canada. [3]Department of Molecular Oncology, British Columbia Cancer Research Centre, Vancouver, British Columbia, Canada. [4]Texas Children's Hospital, Baylor College of Medicine, Houston, TX, USA. [5]Centre for Cell and Gene Therapy, Texas Children's Hospital, Houston Methodist Hospital, Baylor College of Medicine, Houston, TX, USA. [6]Department of Laboratory Medicine and Pathobiology, University of Toronto, Toronto, Ontario, Canada. [7]Department of Medical Biophysics, University of Toronto, Toronto, Ontario, Canada. [8]Division of Haematology/Oncology, Department of Paediatrics, The Hospital for Sick Children, Toronto, Ontario, Canada. [9]Cancer Research Program, McGill University Health Centre Research Institute, Montreal, Quebec, Canada. [10]Brain Tumour Program, Children's Cancer Centre and Department of Paediatrics, Baylor College of Medicine, Houston, TX, USA. [11]Department of Biochemistry & Molecular Biology, Cumming School of Medicine, University of Calgary, Calgary, Alberta, Canada. [12]Charbonneau Cancer Institute, University of Calgary, Calgary, Alberta, Canada. [13]Laboratory of Pathology, National Cancer Institute Centre for Cancer Research, Bethesda, MD, USA. [14]Division of Neurosurgery, Centro Hospitalar Lisboa Norte, Hospital de Santa Maria, Lisbon, Portugal. [15]Department of Pathology and Laboratory Medicine, University of British Columbia, Vancouver, British Columbia, Canada. [16]Division of Neurology, British Columbia Children's Hospital, Vancouver, British Columbia, Canada. [17]Department of Urologic Sciences, University of British Columbia, Vancouver, British Columbia, Canada. [18]Vancouver Prostate Centre, Vancouver Coastal Health Research Institute, Vancouver, British Columbia, Canada. [19]Division of Oncology, Children's Hospital of Philadelphia, Philadelphia, PA, USA. [20]Centre for Childhood Cancer Research, Children's Hospital of Philadelphia, Philadelphia, PA, USA. [21]Perelman School of Medicine, University of Pennsylvania, Philadelphia, PA, USA. [22]Division of Neurosurgery, The Hospital for Sick Children, Toronto, Ontario, Canada. [23]Department of Surgery, Department of Laboratory Medicine and Pathobiology, and Department of Medical Biophysics, University of Toronto, Toronto, Ontario, Canada. ✉e-mail: mdt.cns@gmail.com

emerge, due in part to the lack of targetable somatic single-nucleotide variants in these low mutational burden cancers[3,6]. In addition, most brain tumors are located behind the blood–brain barrier, limiting therapeutic access to the tumor when treatments are given orally or intravenously (i.v.). Interpatient heterogeneity has also limited the development of effective targeted therapies, as there are four molecular subgroups of medulloblastoma[7,8] (consisting of 12 subtypes)[9]. A further nine molecular subgroups of ependymoma also exist[10]. Other treatment barriers include intrapatient heterogeneity, the biological divergence between the primary tumor and metastases and tumor recurrence following treatment[11]. The vast majority of new agent clinical trials are carried out on children with recurrent disease[12], and target maintenance at recurrence is therefore a critical benchmark for therapeutic success. Unlike other primary tumors that recur within the substance of the brain (glioblastoma)[13], both medulloblastoma and ependymoma tend to recur on the surface of the central nervous system or metastasize to the leptomeninges, which are adjacent to, and in both cases bathed by the cerebrospinal fluid (CSF)[5,14]. The location of recurrences adjacent to CSF-containing spaces could be capitalized on as an opportunity for locoregional therapy of recurrent medulloblastoma and ependymoma.

Preliminary preclinical[15,16] and clinical[17,18] results with B7-H3 and GD2-targeting chimeric antigen receptor (CAR) T cells suggest potential therapeutic benefits for the treatment of central nervous system (CNS) malignancies[19–21] with this form of therapy. Of our candidate cell-surface targets, durable regression of HER2$^+$ medulloblastoma cell lines following intratumoral and i.v. injection of HER2$^+$ CAR T cells has been previously observed[22,23]. We hypothesized that we may be able to circumvent interpatient and intrapatient heterogeneity, while also bypassing the blood–brain barrier, through the identification of epitopes consistently present across medulloblastoma and ependymoma subgroups (primary, metastatic and recurrent tumor compartments) and subsequent administration of CAR T cells targeting those epitopes directly into the CSF. Here we evaluate locoregional CSF delivery of CAR T cell therapy as a treatment approach in xenograft mouse models of group 3 metastatic medulloblastoma and PFA ependymoma, the patient subgroups with the highest recurrence rates and for which there are currently limited therapeutic options.

Results

Identification of candidate targets for CAR T cell therapy of group 3 medulloblastoma. To identify candidate targets for CAR T cell therapy of group 3 medulloblastoma, we analyzed microarray data from 763 human medulloblastomas with known subgroup affiliation ($n=70$ WNT; 223 SHH; 144 group 3; 326 group 4)[9] and 9 normal brain control samples ($n=5$ adult cerebellum; 4 fetal cerebellum). Protein targets of CAR T cells enrolled in clinical trials (Supplementary Table 1) were cross referenced with genes highly expressed in primary and recurrent group 3 medulloblastomas. We identified high expression of EPHA2, HER2 and interleukin (IL)-13 receptor α2 (IL-13Rα2), known CAR T cell targets for glioblastoma, in group 3 medulloblastomas in comparison to normal brain controls[19–21,24,25] (Extended Data Fig. 1a–c) and further defined the group 3 subtype-specific expression (group 3α, 3β and 3γ) of these target genes in comparison to normal brain controls (adjusted $P<0.01$; Extended Data Fig. 1d–i). We also observed high protein expression for EPHA2, HER2 and IL-13Rα2 across group 3 primary medulloblastoma (Extended Data Fig. 1j–m) tissue microarrays (TMAs) and matched primary metastatic/recurrent pairs (Extended Data Fig. 2a–c) compared to healthy controls (Extended Data Fig. 1m) and normal compartments of the pediatric developing brain.

As medulloblastoma metastases are known to be biologically divergent from their matched primary tumor[11,26], we compared the expression of EPHA2, HER2 and IL-13Rα2 in human patient samples of group 3 medulloblastoma primary metastatic/recurrent pairs (Extended Data Fig. 2d–j) and found that protein expression levels were maintained within metastases. These data suggested that EPHA2, HER2 and IL-13Rα2 are potential therapeutic targets for upfront primary tumors, metastatic disease and recurrent group 3 medulloblastomas. We subsequently focused on testing EPHA2 monovalent CAR T cells[24], due to EPHA2 having the highest and most conserved protein expression across medulloblastoma samples and trivalent (TRI) CAR T cells[27] as co-targeting HER2, IL-13Rα2 and EPHA2 because TRI CAR T cells have shown success in overcoming interpatient variability in glioblastoma mouse models[25,27].

EPHA2 monospecific and TRI CAR T cells can target primary, metastatic and recurrent group 3 medulloblastoma. Intraventricular delivery of antibody conjugates via CSF has been well tolerated by patients in clinical trials for the treatment of CNS malignancies[28,29]. Cell delivery approaches, specifically intracavity administration to bypass the blood–brain barrier have been tested in patients with metastatic melanoma[30] and with glioblastoma, with success in the latter documented in three patients[17]. Therefore, we sought to determine whether a single dose of intraventricularly delivered CAR T cells administered via the lateral ventricle (LV) could have a potent antitumor effect. We used orthotopic patient-derived cerebellar xenograft (PDX) models of group 3 medulloblastoma (Med114FH, Med411FH and MDT-MMB) transduced with an eGFP-firefly luciferase fusion gene, xenografted into the cerebellum of NOD scid gamma (NSG) mice (Fig. 1a).

A single dose of TRI CAR T cells significantly increased survival versus non-transduced T cells in two out of the three medulloblastoma models (Med114FH, $P<0.05$; Med411FH, $P<0.05$) and a robust survival improvement was seen with a single dose of EPHA2 CAR T cells across all three PDXs (versus no treatment $P<0.005$; versus non-transduced T cells $P<0.005$; Fig. 1b). There was no significant difference observed in survival between EPHA2 CAR and TRI CAR T cell therapy in Med114FH and Med411FH. Non-transduced T cell-treated mice displayed large residual primary tumors postmortem. In contrast, we observed minimal tumor recurrence in the TRI CAR T cell-treated mice (Fig. 1c, Supplementary Fig. 1a,b and Supplementary Fig. 2). Mice treated with either EPHA2 CAR T cells or TRI CAR T cells showed an antitumor response 1 month after therapy; however, tumor recurrences were seen with both treatments. Spinal metastases were only noted following EPHA2 CAR T cell therapy. As the primary tumor regressed following a single round of EPHA2 CAR T cells we believe this allowed time for the tumor to metastasize, hence the eventual recurrence. In comparison, mice treated with non-transduced T cells or TRI CAR T cells showed limited tumor regression following therapy, therefore, mice succumbed to their primary tumor burden before the seeding of associated metastases and time to endpoint was accelerated.

We next evaluated whether repeat therapy with non-transduced T cells, TRI CAR T cells or EPHA2 CAR T cells could extend survival following tumor recurrence (Fig. 2a). On comparison with single-dose-therapy experiments, a second round of non-transduced T cells showed no survival advantage versus a single dose across all three medulloblastoma models. Repeat therapy of TRI CAR T cells versus a single dose of TRI CAR T cells showed a significant increase ($P = 0.024$) in time to endpoint in one-third of the medulloblastoma models. Notably, repeat therapy using EPHA2 CAR T cells resulted in a significant overall survival benefit than a single EPHA2 CAR T cell treatment in medulloblastoma models Med114FH ($P<0.05$) and Med411FH ($P<0.05$) and progression-free survival in model MDT-MMB ($P<0.05$; Fig. 2b). Endpoint H&E staining analysis showed that mice treated with non-transduced T cells or TRI CAR T cells continued to exhibit tumor burden at endpoint (Fig. 2c and Supplementary Figs. 3 and 4). In comparison, following tumor recurrence, a second

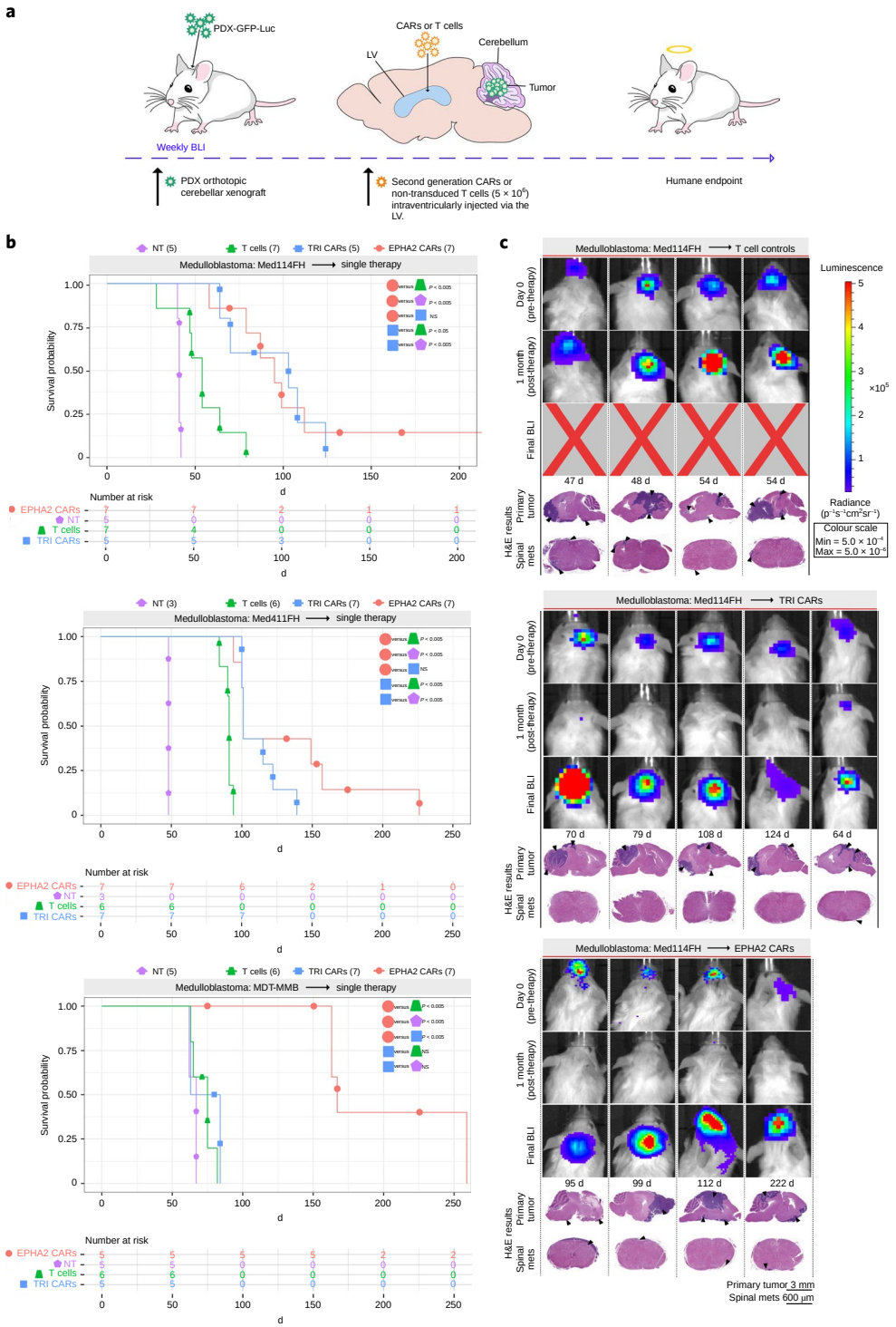

Fig. 1 | CAR T cell therapy improves survival in group 3 medulloblastoma orthotopic xenograft models. a, Experimental scheme. Patient-derived group 3 medulloblastoma cells expressing eGFP-firefly luciferase (PDX-GFP-Luc) were xenografted into NSG mice. BLI was performed to determine orthotopic engraftment, at which point a single dose of 5×10^6 (equivalent to a 20:1 ratio of tumor cells to CAR T cells) monovalent EPHA2 CAR T cells, TRI CAR T cells (EPHA2, HER2 and IL-13Rα2) or non-transduced T cell controls were injected intraventricularly via the LV. Tumor burden was monitored weekly by BLI until a humane endpoint was reached. **b**, Survival analysis of T cell-treated xenografts of Med114FH, Med411FH and MDT-MMB. A two-sided log-rank test with Benjamini–Hochberg procedure was used for analysis, $n=19$ EPHA2 CAR T cells, 19 TRI CAR T cells, 19 non-transduced T cells and 13 no treatment (NT) controls across three independent PDX models. Med114FH: EPHA2 versus T cells $P=0.004$, EPHA2 versus NT $P=0.0025$, EPHA2 versus TRI $P=0.9223$, TRI versus T cells $P=0.0134$, TRI versus NT $P=0.0040$; Med411FH: EPHA2 versus T cells $P=0.002$, EPHA2 versus NT $P=0.004$, EPHA2 versus TRI $P=0.2439$, TRI versus T cells $P=0.0017$, TRI versus NT $P=0.0040$; MDT-MMB: EPHA2 versus T cells $P=0.0062$, EPHA2 versus NT $P=0.0063$, EPHA2 versus TRI $P=0.0062$, TRI versus T cells $P=0.2138$, TRI versus NT $P=0.2709$. NS, not significant. **c**, BLI and final H&E staining analysis of NSG mice xenografted with Med114FH, intraventricularly infused via the LV with non-transduced T cells, TRI CAR T cells or EPHA2 CAR T cells (color map for all images indicates radiance), $n=7$ EPHA2 CAR T cells, 5 TRI CAR T cells, 7 non-transduced T cells and 5 NT biologically independent PDX models. Each column represents one mouse and each row represents a time point, with mouse endpoint (days post-therapy) noted in days.

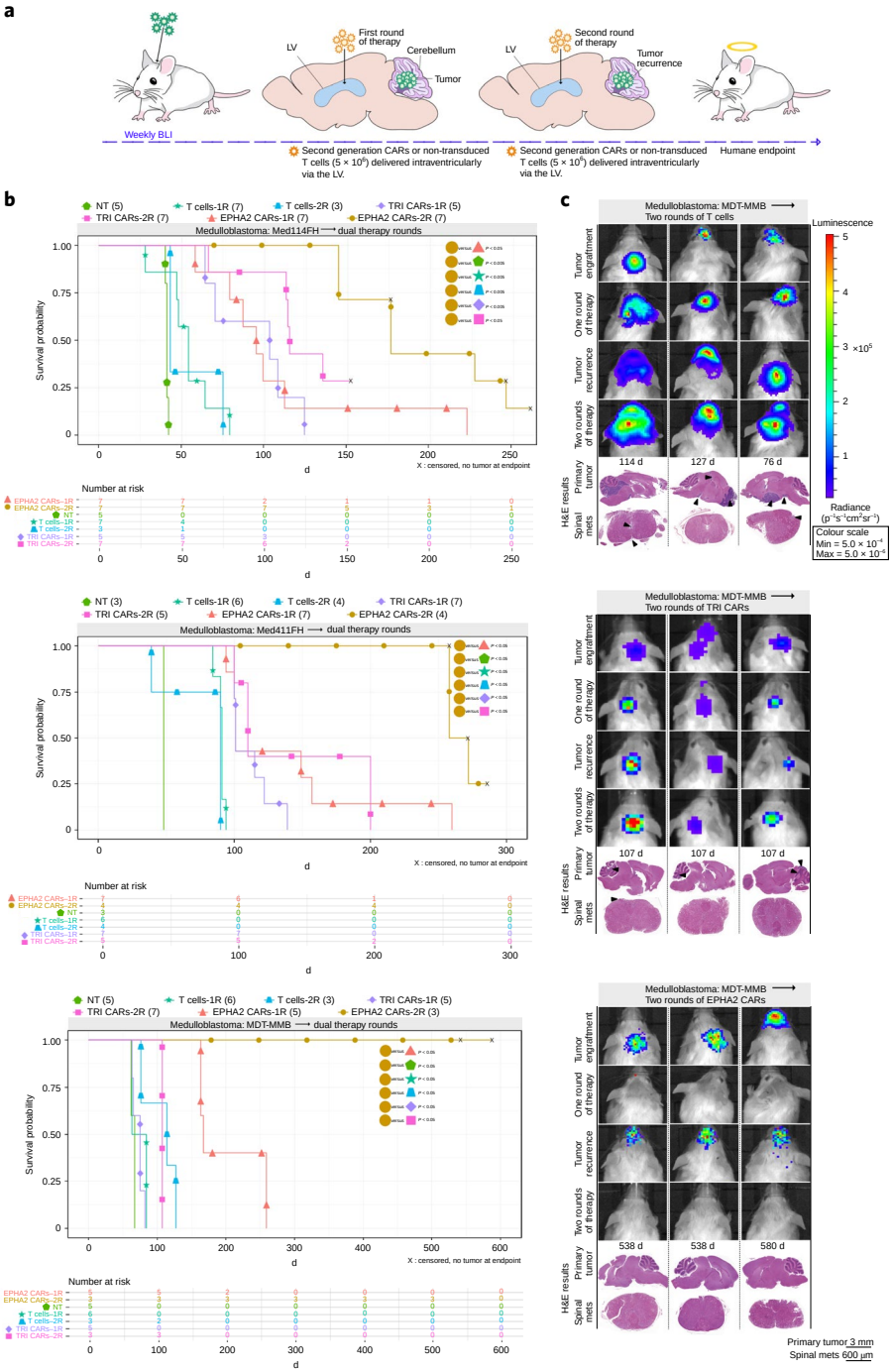

Fig. 2 | Repeat dosing of EPHA2 CAR T cells improves antitumor response in group 3 medulloblastoma orthotopic xenograft models. a, Experimental scheme. Patient-derived group 3 medulloblastoma cells expressing eGFP-firefly luciferase (PDX-GFP-Luc) were xenografted into NSG mice. BLI was performed weekly to determine orthotopic engraftment, at which point a first round of EPHA2 CAR T cells, TRI CAR T cells or non-transduced T cells were administered via the LV. Tumor burden was monitored weekly by BLI until tumor progression or recurrence was observed, wherein a second round of CARs or non-transduced T cells were administered. **b**, Survival analysis of repeat therapy-treated xenografts of Med114FH, Med411FH and MDT-MMB. Data were analyzed by two-sided log-rank test with Benjamini–Hochberg procedure, $n=14$ EPHA2 CAR repeat therapy, 15 TRI CAR repeat therapy and 10 non-transduced T cells repeat therapy across three independent PDX models. Med114FH: EPHA2-one round (1R) versus EPHA2-two rounds (2R), $P=0.0099$; EPHA2-2R versus NT, $P=0.0015$; EPHA2-2R versus T cells-1R, $P=0.0015$; EPHA2-2R versus T cells-2R, $P=0.0032$; EPHA2-2R versus TRI-1R, $P=0.0015$; EPHA2-2R versus TRI-2R, $P=0.0074$. Med411FH: EPHA2-1R versus EPHA2-2R, $P=0.0258$; EPHA2-2R versus NT, $P=0.0200$; EPHA2-2R versus T cells-1R, $P=0.0089$; EPHA2-2R versus T cells-2R, $P=0.00151$; EPHA2-2R versus TRI-1R, $P=0.0071$; EPHA2-2R versus TRI-2R, $P=0.0109$. MDT-MMB: EPHA2-1R versus EPHA2-2R, $P=0.024$; EPHA2-2R versus NT, $P=0.022$; EPHA2-2R versus T cells-1R, $P=0.022$; EPHA2-2R versus T cells-2R, $P=0.022$; EPHA2-2R versus TRI-1R, $P=0.022$; EPHA2-2R versus TRI-2R, $P=0.024$. **c**, BLI and final H&E staining analysis of mice xenografted with MDT-MMB, intraventricularly infused via the LV with two rounds of non-transduced T cells, TRI CAR T cells or EPHA2 CAR T cells (color map indicates radiance), $n=3$ EPHA2-2R CAR T cell, 3 TRI-2R CAR T cell, 3 non-transduced-2R T cell biologically independent PDX models. Each column represents one mouse and each row represents a time point, with mouse endpoint (days post-therapy) noted in days. An 'X' indicates censored mice with no tumor at endpoint.

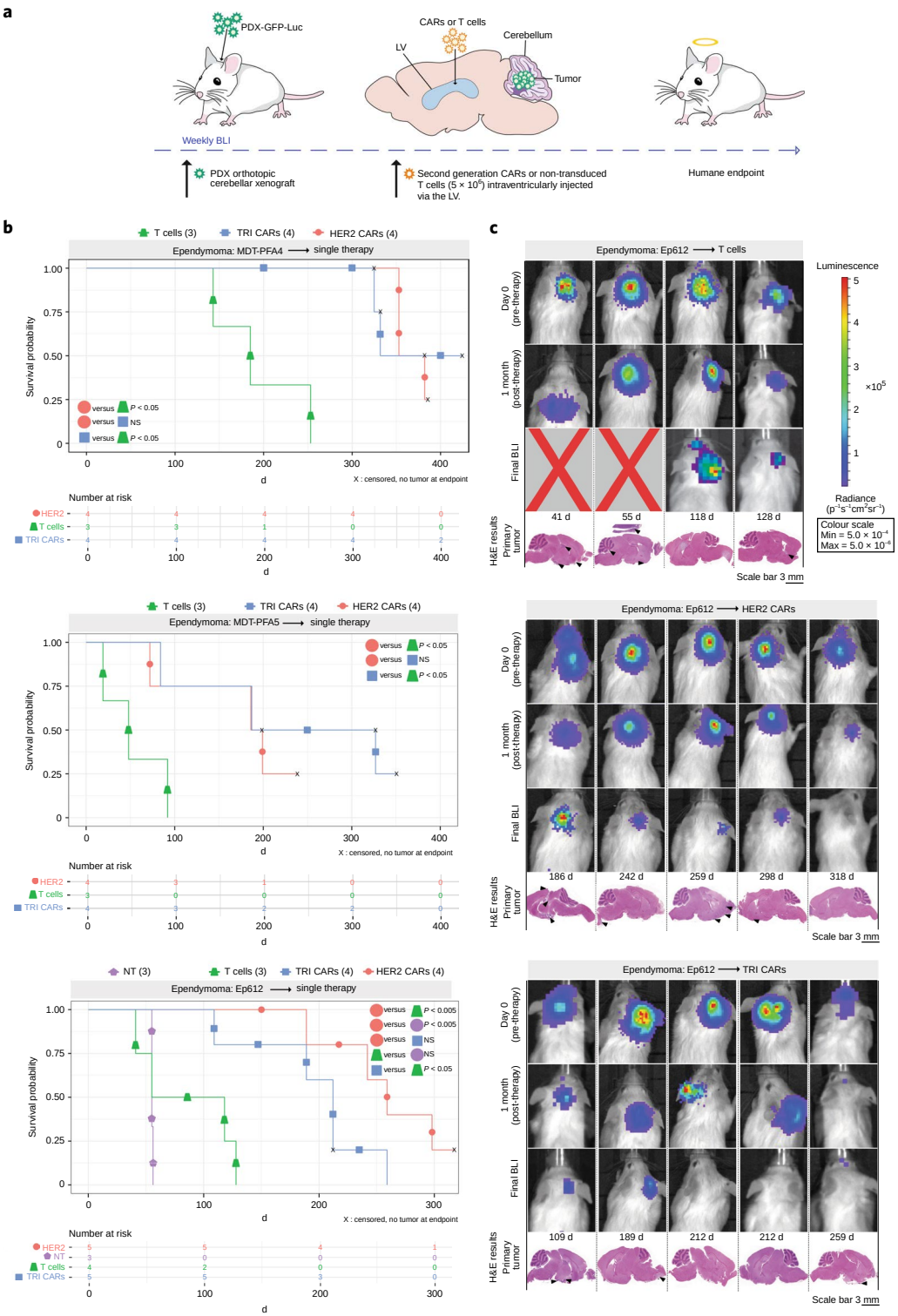

Fig. 3 | HER2 and TRI CAR T cell therapy are effective therapy for PFA ependymoma xenografts. a, Experimental scheme. PFA ependymoma cells expressing eGFP-firefly luciferase (PDX-GFP-Luc) were xenografted into NSG mice. BLI was performed to determine engraftment, at which point a single dose of HER2 CAR T cells, TRI CAR T cells or non-transduced T cells were intraventricularly infused via the LV. Tumor burden was monitored weekly by BLI until endpoint. **b**, Survival analysis of CAR T cell-treated xenografts of MDT-PFA4, MDT-PFA5 and Ep612. Data were analyzed by two-sided log-rank test with Benjamini–Hochberg procedure, $n = 13$ HER2 CAR T cells, 13 TRI CAR T cells and 11 non-transduced T cells across three independent PDX models. MDT-PFA4: HER2 versus T cells, $P = 0.0015$; HER2 versus TRI, $P = 0.508$; TRI versus T cells, $P = 0.015$. MDT-PFA5: HER2 versus T cells, $P = 0.05$; HER2 versus TRI, $P = 0.268$; TRI versus T cells, $P = 0.05$. Ep612: HER2 versus T cells, $P = 0.0092$; HER2 versus TRI, $P = 0.1123$; HER2 versus NT, $P = 0.0092$; TRI versus T cells, $P = 0.0334$; T cells versus NT, $P = 0.4409$. **c**, BLI and H&E staining analysis of NSG mice xenografted with Ep612, intraventricularly infused with non-transduced T cells, HER2 CAR T cells and TRI CAR T cells (color map indicates radiance), $n = 5$ HER CAR T cell, 5 TRI CAR T cell, 4 non-transduced T cell and 3 NT control biologically independent PDX models. Each column represents one mouse and each row represents a time point, with mouse endpoint (days post-therapy) noted in days.

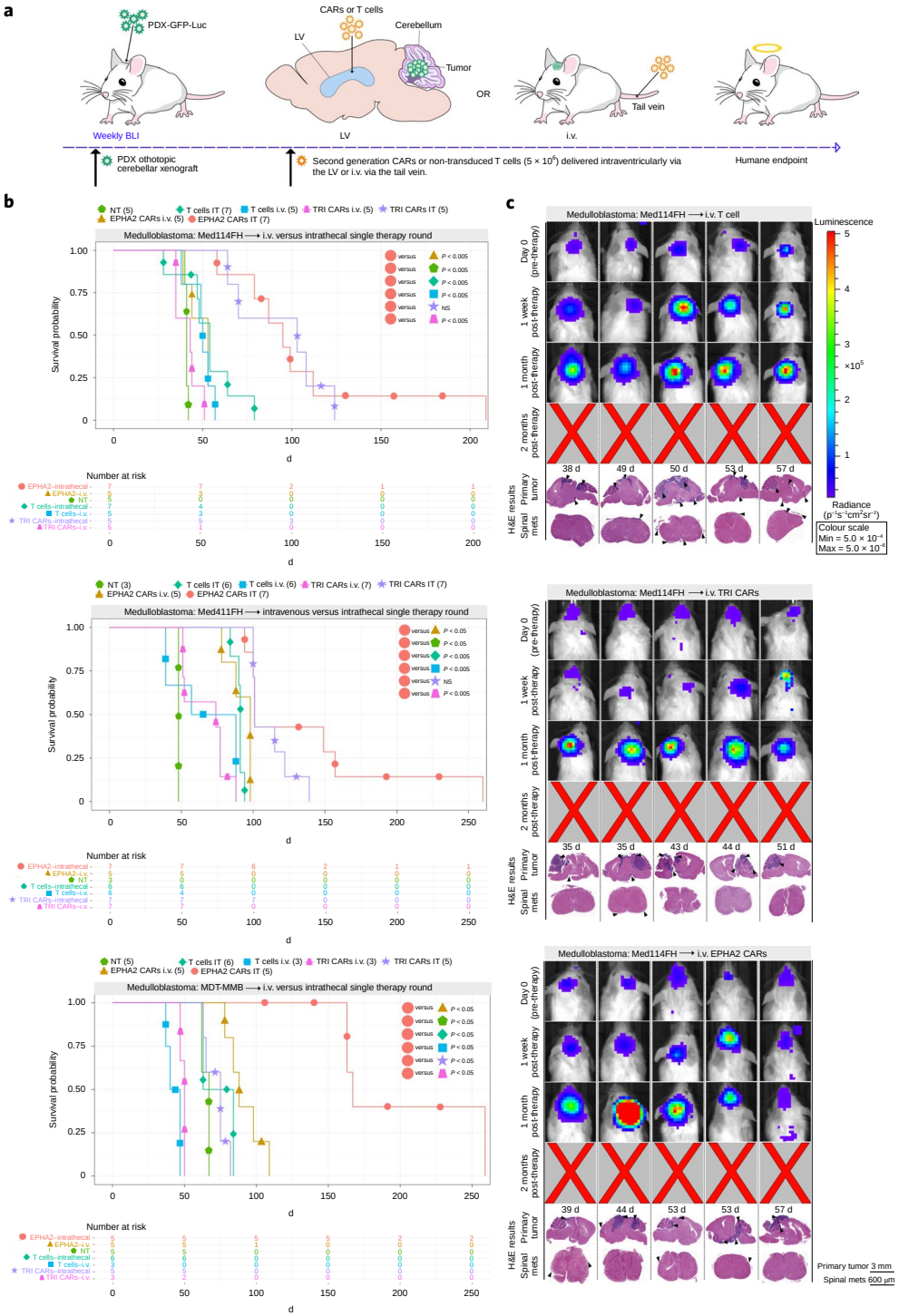

Fig. 4 | LV administration of CAR T cells is superior to i.v. administration for group 3 medulloblastoma orthotopic xenograft models. a, Experimental scheme. Patient-derived group 3 medulloblastoma cells expressing eGFP-firefly luciferase (PDX-GFP-Luc) were xenografted into NSG mice. BLI was performed to determine engraftment, wherein a single dose of EPHA2 CAR T cells, TRI CAR T cells or non-transduced T cells were intraventricularly or i.v. administered. Tumor burden was monitored weekly by BLI until endpoint. **b**, Survival analysis of orthotopic mouse models of Med114FH, Med411FH and MDT-MMB. Data were analyzed by two-sided log-rank test with Benjamini–Hochberg procedure, $n = 15$ i.v. EPHA2 CAR T cells, 15 i.v. TRI CAR T cells and 14 i.v. non-transduced T cells across three independent medulloblastoma PDX models. Med114FH: EPHA2 LV versus EPHA2 i.v., $P = 0.0021$; EPHA2 LV versus NT, $P = 0.0021$; EPHA2 LV versus T cells LV, $P = 0.0048$; EPHA2 LV versus T cells i.v., $P = 0.0021$; EPHA2 LV versus TRI CAR LV, $P = 0.09223$; EPHA2 LV versus TRI CAR i.v., $P = 0.0021$; Med411FH: EPHA2 LV versus EPHA2 i.v., $P = 0.01$; EPHA2 LV versus NT, $P = 0.0052$; EPHA2 LV versus T cells LV, $P = 0.0022$; EPHA2 LV versus T cells i.v., $P = 0.0018$; EPHA2 LV versus TRI LV, $P = 0.2695$; EPHA2 LV versus TRI i.v., $P = 0.0017$. MDT-MMB: EPHA2 LV versus EPHA2 i.v., $P = 0.0076$; EPHA2 LV versus NT, $P = 0.0076$; EPHA2 LV versus T cells LV, $P = 0.0076$; EPHA2 LV versus T cells i.v., $P = 0.0076$; EPHA2 LV versus TRI LV, $P = 0.0076$; EPHA2 LV versus TRI i.v., $P = 0.0094$. IT, intrathecal. **c**, BLI and H&E staining analysis of medulloblastoma PDX model Med114FH, i.v. transfused with non-transduced T cells, TRI CAR T cells, or EPHA2 CAR T cells (color map indicates radiance), $n = 5$ EPHA2 CAR T cell i.v., 5 TRI CAR T cell intravenous and 5 non-transduced T cell i.v. biologically independent PDX models. Each column represents one mouse and each row represents a time point, with mouse endpoint (days post-therapy) noted in days.

infusion of intraventricular EPHA2 CAR T cells into the CSF effectively cleared both the primary and metastatic tumors as demonstrated by bioluminescence imaging (BLI) and endpoint H&E analysis (Fig. 2c and Extended Data Fig. 3b). Immunohistochemical analysis of tumors that recurred identified stable EPHA2 protein expression, suggesting a lack of antigen escape after one or two doses of CAR T cell therapy in this model system (Extended Data Fig. 3a,b). We conclude that intraventricular delivery of CAR T cell therapy is a promising approach for the treatment of both primary and metastatic group 3 medulloblastoma and that repeat administration may provide additional clinical benefit.

Identification of candidate targets for CAR T cell therapy of PFA ependymoma. To identify candidate CAR T cell targets for PFA ependymoma, we analyzed RNA expression profiles from 100 subgroup-specific human ependymoma samples (PFA ($n=54$); spinal cord ($n=15$); and supratentorial (RELA; $n=31$))[31]. Highly expressed genes were cross referenced with CAR T cells currently available for clinical trials[32] identifying the same three differentially expressed genes EPHA2, HER2 and IL-13Rα2 observed in medulloblastoma (Extended Data Fig. 4a–c). We verified that EPHA2, HER2 and IL-13Rα2 were highly expressed at the protein level across ependymoma subgroups using a Canadian multicenter ependymoma TMA (PFA ($n=58$); supratentorial ependymoma (RELA; $n=35$)); spinal ependymoma ($n=11$; Extended Data Figs. 4d–j and 5a–e) with EPHA2 protein expression present in 83 of 84 patients, HER2 protein expression present in 77 of 84 patients and IL-13Rα2 protein expression present in 72 of 84 patients. Protein expression was also verified as stable between pediatric ependymoma primaries and their matched recurrences (Extended Data Fig. 6a–c, versus normal tissue controls Extended Data Fig. 6d–f). In vitro functional co-culture assays used to determine the minimal CAR T cell ratio required to elicit optimal cytotoxic response, corroborated earlier in vivo functional testing (Supplementary Fig. 5a,b). We conclude that EPHA2, HER2 and IL-13Rα2 are potential candidate targets for CAR T cell therapy of PFA ependymoma.

Consequently, we investigated the use of TRI CAR T cells on PFA ependymoma and in parallel we also tested the HER2 monovalent CAR T cell, because HER2 protein expression remained consistent across PFA ependymomas. The antitumor activity of a single LV infusion was determined using PFA ependymoma PDX models (MDT-PFA4, MDT-PFA5 and PFA-Ep612) transduced with an eGFP-firefly luciferase fusion gene, xenografted into the cerebellum of NSG mice (Fig. 3a). HER2 CAR T cell-treated mice showed a significant increase in survival versus non-transduced T cell-treated mice (MDT-PFA4, $P<0.05$; MDT-PFA5, $P<0.05$; Ep612, $P<0.005$), with a parallel therapeutic response observed for TRI CAR T cells versus non-transduced T cell controls (MDT-PFA4, $P<0.05$; MDT-PFA5, $P<0.05$; Ep612, $P<0.05$). No significant difference was observed between monovalent HER2 CAR T cell therapy and TRI CAR T cell therapy in all three PFA ependymoma models (Fig. 3b). All mice treated with non-transduced T cells displayed residual tumor at endpoint. Mice treated with monovalent HER2 CAR T cells showed tumor regression and substantial decrease in tumor burden at endpoint, with one mouse exhibiting no residual tumor at autopsy. TRI CAR T cells showed an antitumor response at 1 month after therapy, with two of five mice tumor-free at endpoint (Fig. 3c and Supplementary Fig. 6). We conclude that intraventricular CAR T cell therapy is a promising therapy for PFA ependymoma.

Comparison of intravenous versus locoregional CSF delivery of CAR T cells. A fundamental factor for the advancement of CAR T cell therapy for brain tumors is the choice of delivery route and whether i.v. or locoregional delivery is more favorable. Studies assessing delivery routes of glioblastoma and breast cancer brain metastases showed that local delivery significantly outperforms i.v. delivery of CAR T cells in orthotopic mouse models[33,34]. To identify the optimal approach for delivery of our candidate CAR T cells, we compared a single dose of i.v. CAR T cell infusions via the tail vein versus LV infusion in three PDX group 3 medulloblastoma models (Med114FH, Med411FH and MDT-MMB; Fig. 4a). The i.v. delivery of monovalent EPHA2 CAR T cells showed a significant increase in survival versus no treatment (Med114FH, $P<0.05$; Med411FH, $P<0.05$; MDT-MMB, $P<0.05$) and a survival advantage versus non-transduced T cells in two of three of the medulloblastoma models (Med114FH, NS; Med411FH, $P<0.05$; MDT-MMB, $P<0.05$). Notably, intraventricular delivery via the LV of monovalent EPHA2 CAR T cells resulted in significant overall survival for all three PDX medulloblastoma models versus i.v. EPHA2 CAR T cells (Med114FH, $P<0.005$; Med411FH, $P<0.05$; MDT-MMB, $P<0.05$; Fig. 4b). Non-transduced T cell-treated mice, TRI CAR T cell and monovalent EPHA2 CAR T cell-treated mice showed no regression in tumor size following i.v. infusion; the mice had large primary cerebellar tumors with extensive infiltration (Fig. 4c and Supplementary Figs. 7 and 8). One of five and three of five mice exhibited spinal metastases following i.v. TRI CAR T cell and monovalent EPHA2 CAR T cell therapy, respectively. Effective tumor clearance and/or delayed progression were not observed after i.v. infusion (Extended Data Fig. 3c).

As the effects of locoregional delivery of CAR T cells via CSF appeared more potent than i.v. infused CAR T cells, we conducted a dose potency study in two medulloblastoma PDXs to determine

Fig. 5 | Azacytidine improves the response to EPHA2 CAR therapy for group 3 medulloblastoma xenografts. a, Experimental scheme. Patient-derived group 3 medulloblastoma cells expressing eGFP-firefly luciferase (PDX-GFP-Luc) were xenografted into NSG mice; 1 week post-xenograft mice began subcutaneous treatment with azacytidine. BLI was performed to determine engraftment, at which point a single dose of EPHA2 CAR T cells, TRI CAR T cells or non-transduced T cells were administered in the LV. Tumor burden was monitored by BLI until endpoint. **b**, Survival analysis of orthotopic mouse models Med114FH and Med411FH treated with azacytidine and intraventricular LV T cell therapy. Data were analyzed by two-sided log-rank test with Benjamini–Hochberg procedure, $n=10$ EPHA2 CAR T cells + azacytidine, 10 TRI CAR T cells + azacytidine and 10 non-transduced T cells + azacytidine, within two independent medulloblastoma PDX models. Med114FH: EPHA2-azacytidine versus EPHA2, $P=0.0047$; EPHA2-azacytidine versus NT, $P=0.0047$; EPHA2-azacytidine versus T cells, $P=0.0047$; EPHA2-azacytidine versus T cells-azacytidine, $P=0.0047$; EPHA2-azacytidine versus TRI, $P=0.0047$; EPHA2-azacytidine versus TRI-azacytidine, $P=0.0047$; EPHA2-azacytidine versus azacytidine only, $P=0.0135$. Med411FH: EPHA2-azacytidine versus EPHA2, $P=0.0036$; EPHA2-azacytidine versus NT, $P=0.0114$; EPHA2-azacytidine versus T cells, $P=0.004$; EPHA2-azacytidine versus T cells-azacytidine, $P=0.005$; EPHA2-azacytidine versus TRI, $P=0.0036$; EPHA2-azacytidine versus TRI-azacytidine, $P=0.0067$; EPHA2-azacytidine versus azacytidine only, $P=0.0073$. **c**, Tumor burden over time expressed as total flux (protons per second) from BLI. $^{***}P<0.0005$, $^{**}P<0.005$, $^{*}P<0.05$ by two-sided one-way analysis of variance (ANOVA) followed by Tukey post hoc test, $n=5$ non-transduced T cell-azacytidine, 6 TRI CAR T cell-azacytidine and 5 EPHA2 CAR T cell-azacytidine biologically independent animals. Day 11: EPHA2 versus T cells/TRI, $P=0$; day 21: EPHA2 versus T cells/TRI, $P=0$; day 35: EPHA2 versus T cells/TRI, $P=0$. **d**, BLI and H&E analysis of PDX Med114FH, treated with azacytidine and LV infusion with non-transduced T cells, TRI CAR T cells or EPHA2 CAR T cells (color map indicates radiance), $n=5$ EPHA2-azacytidine, 6 TRI CAR-azacytidine and 5 non-transduced T cell-azacytidine biologically independent PDX models. Each column represents one mouse and each row represents a time point, mouse endpoint (days post-therapy) noted in days.

the minimal dose required to exert tumor clearance via two different routes of administration (Extended Data Fig. 7a,b). No differences in survival or tumor burden were observed between the two delivery routes from 5×10^6 to 10×10^6 non-transduced (Supplementary Figs. 8 and 9) or TRI CAR T‹cells (Supplementary Figs. 10 and 11) between the two delivery routes. However, tumor burden

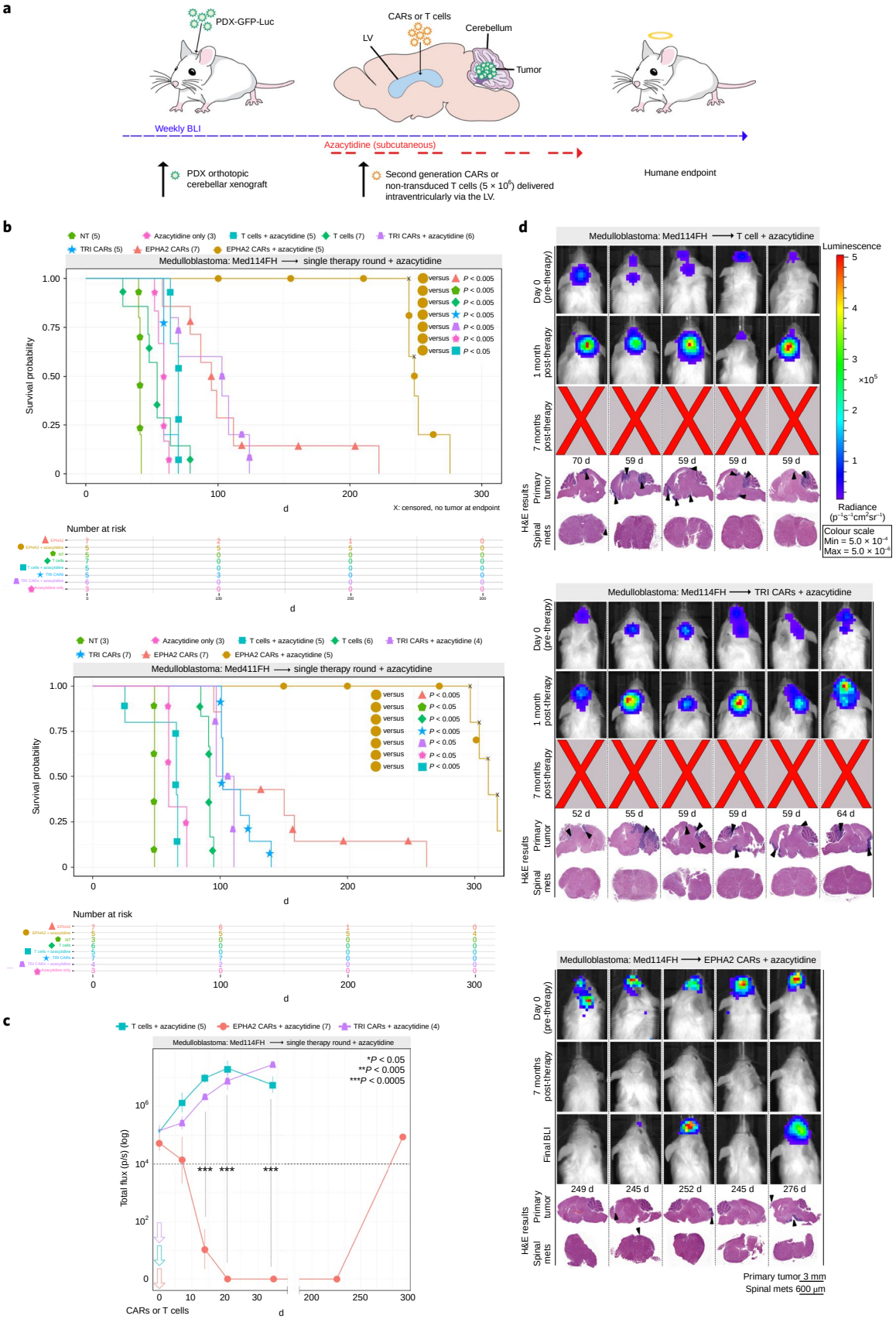

significantly decreased when treated with EPHA2 CAR T cells LV (Extended Data Figs. 8a and 9a) versus i.v. delivery (Extended Data Figs. 8b and 9b) at doses of 5×10^6 or 10×10^6 (Med114FH, $P<0.0005$, $P<0.0005$; Med411FH, $P<0.0005$, $P<0.05$, respectively). Because the lower dose of 2.5×10^6 EPHA2 CAR T cells was not seen to effectively clear the tumor burden, we determined the lowest optimal dose to therefore be 5×10^6 CAR T cells (Extended Data Figs. 8c and 9c). Longitudinal analysis of CSF and blood collected at humane or defined endpoint showed an increase in IL-23 release, a cytokine that plays a critical role in establishing inflammatory immunity and an enhanced T cell-activation state[35] in intraventricularly infused mice, regardless of CAR or non-transduced T cells being delivered, suggesting an enhanced state of T cell activation due to the increased proximity of T cells to the tumor site (Extended Data Fig. 10a; i.v. versus intraventricular CSF delivery, $P<0.05$). Granulocyte–macrophage colony-stimulating factor cytokine, an essential regulator of T cell activation[36], was consistently secreted across all treatment groups. Except for IL-15 (a serum cytokine)[37], which was seen within all blood serum samples, no other distinct patterns of cytokine activity were observed between delivery routes and dose escalations. T cell accumulation was seen only in mice infused LV with EPHA2 CAR T cells (Extended Data Fig. 10b,c). Therefore, while i.v. delivery of CAR T cells demonstrates some activity, intraventricular administration of EPHA2-targeting CAR T cells (not TRI CAR T cells) delivers superior therapeutic outcomes in our group 3 medulloblastoma in vivo models. Intraventricular CSF delivery allows direct CAR T cell access to the tumor site and concomitant increased maintenance of CAR T cell activation as a result.

Monovalent CAR T cell conformation is superior in an EPHA2-rich environment. In previous work, T cells with multiple CARs have typically proved more efficacious than their monovalent CAR T cell counterparts. Computational modeling and docking of HER2 (Supplementary Fig. 12a), IL-13Rα2 (Supplementary Fig. 12b) and EPHA2 (Supplementary Fig. 12c,d) CARs to their receptors was performed to better understand the efficacy differences observed between the monovalent and TRI CAR T cells. Two models for EPHA2 CAR were generated from SWISSMODEL, a monomer and a homodimer. Dimeric EPHA2 CAR allows for docking of two EPHA2 receptors (Supplementary Fig. 12e,f), which may result in overall decreased activity of TRI CAR T cells versus monomeric EPHA2 CAR T cells due to steric constraints at the immune synapse (Supplementary Fig. 12g,h).

To address the significant differences in CAR T cell efficacy between monovalent EPHA2 CAR T cells and TRI CAR T cells, we conducted in vivo composite mix analysis (Supplementary Fig. 13a). We found a composite mixture of CAR T cells to be inferior to monovalent EPHA2 CAR T cells ($P=0.0003$, Cox proportional hazard). Notably, we also saw a marked decrease in survival in comparison to TRI CAR T cells ($P=0.03$, log-rank test with Benjamini–Hochberg procedure). We believe this decrease in survival is due to the overall decrease in candidate CAR T cell numbers administered via the composite mixture; for example, the EPHA2–HER2–IL-13Rα2 mixture contained candidate CAR T cell ratios of 1.6×10^6 to 1.6×10^6 to 1.6×10^6 to give a total number of 5×10^6. We conclude that TRI CAR T cells, while inferior to monovalent EPHA2 CAR T cells, remain superior to a composite mixture of CAR T cells.

EPHA2 monovalent CAR T cells synergize with azacytidine to significantly improve overall survival for group 3 medulloblastoma. While EPHA2 CAR T cells are efficacious to a certain degree, tumor recurrences were observed and we therefore sought to improve this therapy with a combination-therapy approach. One mechanism of failure or suboptimal response to CAR T cell therapy is antigenic escape secondary to epigenetic silencing of the gene targeted by CAR T cells[38]. Azacytidine is a well-documented hypomethylating agent and effective chemotherapeutic agent for acute myelogenous leukemia[39,40]. Through covalent trapping of DNA methyltransferase in genomic DNA and subsequent hypomethylation, azacytidine acts to induce cell death in cancer cells reliant on epigenetic silencing[14,41] and transiently increases expression of tumor-associated antigens[42,43]. Furthermore, various immunomodulatory effects of azacytidine have been well documented, including sensitization of tumor cells to cytotoxic $CD8^+$ T cells[43,44] and stimulated expansion of regulatory $CD4^+$ T cells and $CD8^+$ cytotoxic T cells[45]. To determine whether epigenetic silencing was playing a role in treatment failure, we tested the synergistic role of the DNA demethylating agent azacytidine in combination with CAR T cells[46–49].

Medulloblastoma cells (Med114FH and Med411FH) tagged with eGFP-firefly luciferase were xenografted into the cerebellum of NSG mice. At 1 week after xenograft, mice began subcutaneous azacytidine treatment (Fig. 5a). CAR T cells were administered when orthotopic engraftment was confirmed by BLI. Monovalent EPHA2 CAR T cells in combination with azacytidine revealed a striking and significant survival advantage versus monovalent EPHA2 CAR T cells alone (Med114FH, $P<0.005$; Med411FH, $P<0.005$). In comparison to EPHA2 combination CAR T cell therapy, azacytidine in combination with TRI CAR T cells (Med114FH, $P<0.005$; Med411FH, $P<0.05$) and azacytidine plus non-transduced T cells

Fig. 6 | Combined azacytidine and CAR T cell therapy improves progression-free survival in PFA ependymoma orthotopic xenograft models. **a**, Experimental scheme. PFA ependymoma cells expressing eGFP-firefly luciferase (PDX-GFP-Luc) were xenografted into NSG mice; 1 week post-xenograft mice began subcutaneous treatment of azacytidine. Following BLI to determine engraftment, HER2 CAR T cells, TRI CAR T cells or non-transduced T cells were intraventricularly administered by the LV. Tumor burden was monitored weekly by BLI until endpoint. **b**, Survival analysis of combined azacytidine and T cell-treated orthotopic xenografts of MDT-PFA4, MDT-PFA5 and Ep612. Data were analyzed by two-sided log-rank test with Benjamini–Hochberg procedure, $n=12$ non-transduced T cells + azacytidine, 23 TRI CAR T cells + azacytidine and 18 HER2 CAR T cells + azacytidine across three independent PDX models. MDT-PFA4: HER2-azacytidine versus HER2, $P=0.0017$; HER2-azacytidine versus T cells, $P=0.00305$; HER2-azacytidine versus T cells-azacytidine, $P=0.00110$; HER2-azacytidine versus TRI, $P=0.99$; HER2-azacytidine versus TRI-azacytidine, $P=0.00011$; TRI-azacytidine versus HER2, $P=0.00029$; TRI-azacytidine versus T cells, $P=0.00061$; TRI-azacytidine versus T cells-azacytidine, $P=0.00025$; TRI-azacytidine versus TRI, $P=0.00029$. MDT-PFA5: HER2-azacytidine versus HER2, $P=0.008$; HER2-azacytidine versus T cells, $P=0.011$; HER2-azacytidine versus T cells-azacytidine, $P=0.008$; HER2-azacytidine versus TRI, $P=0.542$; HER2-azacytidine versus TRI-azacytidine, $P=0.874$; TRI-azacytidine versus HER2, $P=0.008$; TRI-azacytidine versus T cells, $P=0.008$; TRI-azacytidine versus T cells-azacytidine, $P=0.008$; TRI-azacytidine versus TRI, $P=0.737$. Ep612: HER2-azacytidine versus HER2, $P=0.84$; HER2-azacytidine versus NT, $P=0.007$; HER2-azacytidine versus T cells, $P=0.00622$; HER2-azacytidine versus T cells-azacytidine, $P=0.00622$; HER2-azacytidine versus TRI, $P=0.00622$; HER2-azacytidine versus TRI-azacytidine, $P=0.00723$; TRI-azacytidine versus HER2, $P=0.00622$; TRI-azacytidine versus NT, $P=0.0082$; TRI-azacytidine versus T cells, $P=0.00071$; TRI-azacytidine versus T cells-azacytidine, $P=0.00071$; TRI-azacytidine versus TRI, $P=0.00071$. **c**, BLI and H&E staining analysis of NSG mice xenografted with Ep612, treated with azacytidine and intraventricularly infused with non-transduced T cells, HER2 CAR T cells or TRI CAR T cells (color map indicates radiance), $n=5$ HER2-azacytidine, 6 TRI-azacytidine and 4 T cell-azacytidine biologically independent PDX models. Each column represents one mouse and each row represents a time point, mouse endpoint (days post-therapy) noted in days.

(Med114FH, $P < 0.005$; Med411FH, $P < 0.005$) (Fig. 5b). Azacytidine treatment alone provided no survival advantage versus non-transduced T‹ cells alone for two group 3 medulloblastomas (Med114FH, NS; Med411FH, $P = 0.005$); Med411FH displayed a significant survival with non-transduced T‹cells versus azacytidine alone. The combination of EPHA2 monovalent CAR T‹cells with

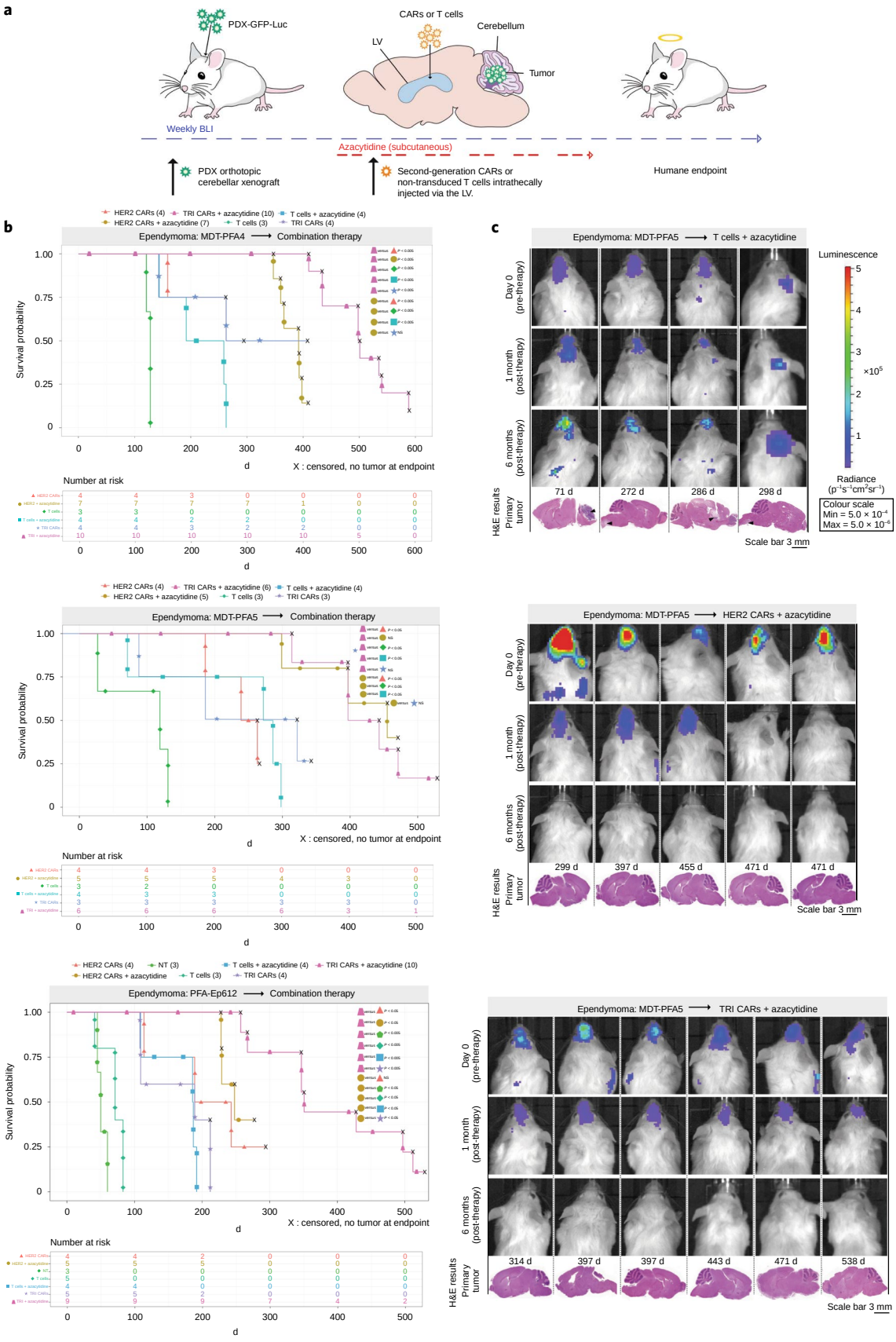

azacytidine resulted in a significant decrease in tumor burden (Fig. 5c), with complete tumor clearance and progression-free survival observed in two of five mice, reaching endpoint due to old age at 245 d and 249 d, respectively (Fig. 2d and Supplementary Fig. 13b). A significant increase in EPHA2 antigen expression following in vitro azacytidine treatment was observed in all three of the medulloblastoma PDXs (Med114FH, $P < 0.001$; Med411FH, $P < 0.01$; MDT-MMB, $P < 0.001$; Supplementary Fig. 14), potentially accounting for this overall survival advantage. All mice showed significant tumor regression 7 months after therapy, with three displaying small primary tumors at final endpoint. Mice receiving combined TRI CAR T cells or non-transduced T cell therapy showed large primary cerebellar tumors and no regression in overall tumor size 1 month after therapy by BLI. We conclude that the combination of azacytidine with locoregional LV CAR T cell therapy may offer additional benefits to patients with group 3 medulloblastoma.

Combination CAR T cell and azacytidine for therapy of PFA ependymomas. To determine whether azacytidine demonstrates synergy with HER2 monovalent or TRI CAR T cell therapy for PFA ependymoma, PDXs (MDT-PFA4, MDT-PFA5, PFA-Ep612) tagged with eGFP-firefly luciferase were xenografted into the cerebellum of NSG mice and at 1 week post-xenograft, mice began subcutaneous azacytidine treatment (Fig. 6a). CAR T cells were administered when orthotopic engraftment was confirmed by BLI. Mice receiving combined HER2 monovalent CAR T cells and azacytidine therapy exhibited a significant survival improvement versus mice receiving non-transduced T cells plus azacytidine in all three ependymoma PDX models (MDT-PFA4, $P < 0.05$; MDT-PFA5, $P < 0.05$; Ep612, $P < 0.005$). TRI CAR T cells combined with azacytidine therapy revealed a similar significant therapeutic response versus non-transduced T cells and azacytidine (MDT-PFA4, $P < 0.05$; MDT-PFA5, $P < 0.05$; Ep612, $P < 0.005$). Only the Ep612 PFA line displayed a significant survival benefit between HER2 CAR T cells compared to TRI CAR T cells with azacytidine ($P < 0.05$; Fig. 6b). The combined epigenetic modifier and immunotherapeutic approach showed the highest antitumor efficacy in all three PFA ependymoma models, with progression-free survival and effective tumor clearance observed in every mouse enrolled (Fig. 6c and Supplementary Fig. 15). As observed with medulloblastoma, the addition of azacytidine to CAR T cell therapy improves survival and synergy, representing a promising therapy for PFA ependymoma.

Discussion

We found that a plurality of group 3 medulloblastomas have elevated protein expression of EPHA2, IL-13Rα2 and, to a lesser extent, HER2, suggesting that these proteins may serve as good targets for CAR T cell therapies. The limited positive expression of HER2 in the medulloblastoma PDX models used within our study replicates the limited expression levels we observed within the TMAs and paired primary metastases/recurrent tumor samples of group 3 medulloblastoma. We have demonstrated the efficacy of locoregional CSF delivery of EPHA2 monovalent, HER2 monovalent and TRI (EPHA2–HER2–IL-13Rα2) CAR T cell therapy in multiple PDX models of medulloblastoma and ependymoma. Group 3 medulloblastoma primary and recurrent samples have an environment rich in EPHA2 receptors. Conversely, in ependymomas, EPHA2, HER2 and IL-13Rα2 receptors seem to have similar protein expression levels in the primary and recurrent tumor compartments. In this case, there is equal opportunity for the EPHA2, HER2 and IL-13Rα2 CARs to bind. As the monovalent EPHA2 CAR T cell significantly outperforms the TRI CAR T cell in an EPHA2 environment, the use of the EPHA2 monovalent CAR T cells would be deemed the most appropriate for use in future group 3 medulloblastoma clinical trials. In comparison, we believe the use of TRI CAR T cells would be deemed most appropriate for effective treatment of PFA ependymomas in future clinical trials.

Our data suggest that repeat administration of CAR T cells, perhaps through an Ommaya reservoir (an intraventricular catheter used for aspiration of CSF and for delivery of drugs into the CSF), could increase the efficacy of therapy compared to either i.v. administration or single-dose intraventricular administration via the LV. Delivery of CAR T cell therapy directly into the CSF likely increases the exposure of CAR T cells to cancer cells and might decrease systemic toxicity and attenuate on-target, off-tumor effects. EPHA2, HER2 and IL-13Rα2 display little to no protein expression in normal developing brain samples; however, the targets do show protein expression in normal tissues samples, namely the spleen, thymus and pancreas. Although systemic toxicity was not assessed in our study (and is a line of future experimental inquiry), clinical and safety data for HER2 and IL-13Rα2 CAR T cells already exist and no dose-limiting toxicity has been observed[17,20]. Furthermore, EPHA2 CAR T cell analysis is an ongoing assessment[50] in the locoregional delivery of CAR T cells for EPHA2-positive malignant gliomas. Locoregional delivery of CAR T cells directly into the CSF may reduce the risk of systemic toxicities associated with CAR T cells, in comparison to the more commonly used i.v. delivery approach. In clinical trials of HER2 and EGFRvIII[51,52] CAR T cells, i.v. infusion of CAR T cells increased the risk of pulmonary toxicities and in some cases were fatal[51,52]. Thus, locoregional delivery is anticipated to reduce systemic toxicities and to be broadly relevant for treatment of CNS neoplasms[53].

Our data from both the group 3 medulloblastoma and PFA ependymoma models clearly show a synergy between intraventricular CSF CAR T cell therapy and the DNA demethylating agent azacytidine. It is unclear whether the effects of azacytidine are tumor cell autonomous and immunotherapy-independent, tumor cell autonomous and potentiating the immunotherapy (that is, avoidance or reversal of tumor epitope silencing) and/or immune cell-related. Exploring the mechanism underpinning azacytidine efficacy will represent the focus of future experiments. Epigenetic priming with azacytidine may represent an effective neoadjuvant therapeutic approach when complemented with CAR T cell therapy.

The anatomic location of the vast majority of group 3 medulloblastoma and PFA ependymoma recurrences, adjacent to and bathed by the CSF, and the almost complete lack of targeted agents currently being tested in clinical trials represent an opportunity for the effective, direct and full delivery of EPHA2 monovalent or TRI CAR T cells in combination with azacytidine as effective therapeutic modalities for group 3 medulloblastoma and PFA ependymoma primary and recurrences, respectively.

Online content

Any methods, additional references, Nature Research reporting summaries, source data, extended data, supplementary information, acknowledgements, peer review information; details of author contributions and competing interests; and statements of data and code availability are available at https://doi.org/10.1038/s41591-020-0827-2.

Received: 16 July 2019; Accepted: 6 March 2020;
Published online: 27 April 2020

References

1. Pui, C. H., Gajjar, A. J., Kane, J. R., Qaddoumi, I. A. & Pappo, A. S. Challenging issues in pediatric oncology. *Nat. Rev. Clin. Oncol.* **8**, 540–549 (2011).
2. Vladoiu, M. C. et al. Childhood cerebellar tumors mirror conserved fetal transcriptional programs. *Nature* **572**, 67–73 (2019).
3. Mack, S. C. et al. Therapeutic targeting of ependymoma as informed by oncogenic enhancer profiling. *Nature* **553**, 101–105 (2018).
4. Khatua, S., Ramaswamy, V. & Bouffet, E. Current therapy and the evolving molecular landscape of paediatric ependymoma. *Eur. J. Cancer* **70**, 34–41 (2017).

5. Ramaswamy, V. et al. Recurrence patterns across medulloblastoma subgroups: an integrated clinical and molecular analysis. *Lancet Oncol.* **14**, 1200–1207 (2013).
6. Northcott, P. A. et al. The whole-genome landscape of medulloblastoma subtypes. *Nature* **547**, 311–317 (2017).
7. Taylor, M. D. et al. Molecular subgroups of medulloblastoma: the current consensus. *Acta Neuropathol.* **123**, 465–472 (2011).
8. Northcott, P. A et al. Medulloblastoma comprises four distinct molecular variants. *J. Clin. Oncol.* **29**, 1408–1414 (2011).
9. Cavalli, F. M. et al. Intertumoral heterogeneity within medulloblastoma subgroups. *Cancer Cell* **31**, 737–754 (2017).
10. Kulozik, A. E. et al. Molecular classification of ependymal tumors across all CNS compartments, histopathological grades, and age groups. *Cancer Cell* **27**, 728–743 (2015).
11. Morrissy, A. S. et al. Divergent clonal selection dominates medulloblastoma at recurrence. *Nature* **529**, 351–357 (2016).
12. Garzia, L. et al. A hematogenous route for medulloblastoma leptomeningeal metastases. *Cell* **172**, 1050–1062 (2018).
13. Bette, S. et al. Retrospective analysis of radiological recurrence patterns in glioblastoma, their prognostic value and association to postoperative infarct volume. *Sci. Rep.* **8**, 1–12 (2018).
14. Mack, S. C. et al. Epigenomic alterations define lethal CIMP-positive ependymomas of infancy. *Nature* **506**, 445–450 (2014).
15. Majzner, R. G. et al. CAR T cells targeting B7-H3, a pan-cancer antigen, demonstrate potent preclinical activity against pediatric solid tumors and brain tumors. *Clin. Cancer Res.* **25**, 2560–2574 (2019).
16. Mount, C. W et al. Potent antitumor efficacy of anti-GD2 CAR T cells in H3-K27M^{+} diffuse midline gliomas. *Nat. Med.* **24**, 572–579 (2018).
17. Brown, C. E et al. Bioactivity and safety of IL13Rα2-redirected chimeric antigen receptor CD8+ T cells in patients with recurrent glioblastoma. *Clin. Cancer Res.* **21**, 4062–4072 (2105).
18. Keu, K. V. et al. Reporter gene imaging of targeted T cell immunotherapy in recurrent glioma. *Sci. Transl. Med.* **9**, eaag2196 (2017).
19. Brown, C. E. et al. Regression of glioblastoma after chimeric antigen receptor T cell therapy. *N. Engl. J. Med.* **375**, 2561–2569 (2016).
20. Ahmed, N. et al. HER2-specific chimeric antigen receptor-modified virus-specific T cells for progressive glioblastoma. *JAMA Oncol.* **3**, 1094 (2017).
21. O'Rourke, D. M. et al. A single dose of peripherally infused EGFRvIII-directed CAR T cells mediates antigen loss and induces adaptive resistance in patients with recurrent glioblastoma. *Sci. Transl. Med.* **9**, eaaa0984 (2017).
22. Ahmed, N. et al. Regression of experimental medulloblastoma following transfer of HER2-specific T cells. *Cancer Res.* **67**, 5957–5964 (2007).
23. Nellan, A. et al. Durable regression of medulloblastoma after regional and intravenous delivery of anti-HER2 chimeric antigen receptor T cells. *J. Immunother. Cancer* **6**, 30 (2018).
24. Chow, K. K. et al. T cells redirected to EphA2 for the immunotherapy of glioblastoma. *Mol. Ther.* **21**, 629–637 (2013).
25. Krebs, S. et al. T cells redirected to interleukin-13Rα2 with interleukin-13 mutein-chimeric antigen receptors have anti-glioma activity but also recognize interleukin-13Rα1. *Cytotherapy* **16**, 1121–1131 (2014).
26. Wu, X. et al. Clonal selection drives genetic divergence of metastatic medulloblastoma. *Nature* **482**, 529–533 (2012).
27. Bielamowicz, K. et al. Trivalent CAR T cells overcome interpatient antigenic variability in glioblastoma. *Neuro. Oncol.* **20**, 506–518 (2018).
28. Schulz, H. et al. Intraventricular treatment of relapsed central nervous system lymphoma with the anti-CD20 antibody rituximab. *Haematologica* **89**, 753–754 (2004).
29. Kramer, K. et al. A phase II study of radioimmunotherapy with intraventricular 131I-3F8 for medulloblastoma. *Pediatr. Blood Cancer* **65**, (2018).
30. Hwu, P. Lymphodepletion plus adoptive cell transfer with or without dendritic cell immunization in patients with metastatic melanoma. ClinicalTrials.gov Identifier: NCT00338377 (2006).
31. Witt, H. et al. Delineation of two clinically and molecularly distinct subgroups of posterior fossa ependymoma. *Cancer Cell* **20**, 143–157 (2011).
32. Morrissy, A. S. et al. Spatial heterogeneity in medulloblastoma. *Nat. Genet.* **49**, 780–788 (2017).
33. Priceman, S. J. et al. Regional delivery of chimeric antigen receptor-engineered T cells effectively targets HER2^{+} breast cancer metastasis to the brain. *Clin. Cancer Res.* **24**, 95–105 (2018).
34. Brown, C. E. et al. Optimization of IL13Rα2-targeted chimeric antigen receptor T cells for improved anti-tumor efficacy against glioblastoma. *Mol. Ther.* **26**, 31–44 (2018).
35. Stritesky, G. L., Yeh, N. & Kaplan, M. H. IL-23 promotes maintenance but not commitment to the Th17 lineage. *J. Immunol.* **181**, 5948–5955 (2008).
36. Rasouli, J. et al. Expression of GM-CSF in T cells is increased in multiple sclerosis and suppressed by IFN-β therapy. *J. Immunol.* **194**, 5085–5093 (2015).
37. Bergamaschi, C. et al. Circulating IL-15 exists as heterodimeric complex with soluble IL-15Rα in human and mouse serum. *Blood* **120**, e1–8 (2012).
38. Hegde, M. et al. Tandem CAR T cells targeting HER2 and IL-13Rα2 mitigate tumor antigen escape. *J. Clin. Invest.* **126**, 3036–3052 (2016).
39. Momparler, R. L., Côté, S., Momparler, L. F. & Idaghdour, Y. Epigenetic therapy of acute myeloid leukemia using 5-aza-2′-deoxycytidine (decitabine) in combination with inhibitors of histone methylation and deacetylation. *Clin. Epigenetics* **6**, 19 (2014).
40. Montalban-Bravo, G. & Garcia-Manero, G. Myelodysplastic syndromes: 2018 update on diagnosis, risk-stratification and management. *Am. J. Hematol.* **93**, 129–147 (2018).
41. Stresemann, C. & Lyko, F. Modes of action of the DNA methyltransferase inhibitors azacytidine and decitabine. *Int. J. Cancer* **123**, 8–13 (2008).
42. Qiu, X. et al. Equitoxic doses of 5-azacytidine and 5-aza-2'deoxycytidine induce diverse immediate and overlapping heritable changes in the transcriptome. *PLoS ONE* **5**, (2010).
43. Gang, A. O. et al. 5-azacytidine treatment sensitizes tumor cells to T cell mediated cytotoxicity and modulates NK cells in patients with myeloid malignancies. *Blood Cancer J.* **4**, e197 (2014).
44. Goodyear, O. C. et al. Azacitidine augments expansion of regulatory T cells after allogeneic stem cell transplantation in patients with acute myeloid leukemia (AML). *Blood* **119**, 3361–3369 (2012).
45. Fozza, C. et al. Azacitidine improves the T cell repertoire in patients with myelodysplastic syndromes and acute myeloid leukemia with multilineage dysplasia. *Leuk. Res.* **39**, 957–963 (2015).
46. Mokhtari, R. B. et al. Combination therapy in combating cancer. *Oncotarget* **8**, 38022–38043 (2017).
47. Rodríguez-Paredes, M. & Esteller, M. Cancer epigenetics reaches mainstream oncology. *Nat. Med.* **17**, 330–339 (2011).
48. Terracina, K. P. et al. DNA methyltransferase inhibition increases efficacy of adoptive cellular immunotherapy of murine breast cancer. *Cancer Immunol. Immunother.* **65**, 1061–1073 (2016).
49. Quddus, J. et al. Treating activated CD4^{+} T cells with either of two distinct DNA methyltransferase inhibitors, 5-azacytidine or procainamide, is sufficient to cause a lupus-like disease in syngeneic mice. *J. Clin. Invest.* **92**, 38–53 (1993).
50. Niu, L. CAR T cell immunotherapy for EphA2-positive malignant glioma patients. ClinicalTrials.gov Identifier: NCT02575261 (2017).
51. Goff, S. L. et al. Pilot trial of adoptive transfer of chimeric antigen receptor-transduced T cells targeting EGFRvIII in patients with glioblastoma. *J. Immunother.* **42**, 126–135 (2019).
52. Morgan, R. A. et al. Case report of a serious adverse event following the administration of T cells transduced with a chimeric antigen receptor recognizing ERBB2. *Mol. Ther.* **18**, 843–851 (2010).
53. Akhavan, D. et al. CAR T cells for brain tumors: lessons learned and road ahead. *Immunol. Rev.* **290**, 60–84 (2019).

Methods

Immunohistochemistry analysis and H scores. *IHC on human tissue microarrays.* Formalin-fixed, paraffin-embedded TMA sections were analyzed for IL-13RA2, HER2/CB11 and EPHA2 protein expression. All immunohistochemistry (IHC) was performed using the Ventana Discovery platform. IHC was optimized and performed with IL-13RA2 (Abcam GR270853), HER2/CB11 (BioGenex MU134C) and EPHA2 (Abnova MAB1769) with dilutions of 1:200, 1:400 and 1:500, respectively. In brief, tissue sections were incubated in Tris EDTA buffer (cell conditioning 1; CC1 standard) at 95 °C for 1 h to retrieve antigenicity, followed by incubation with the respective primary antibody for 1 h. Bound primary antibodies were incubated with the respective secondary antibodies (Jackson Laboratories) at 1:500 dilution, followed by Ultramap HRP and Chromomap DAB detection (Roche). For staining optimization and to control for staining specificity, normal organs were used as negative and positive controls (see Extended Data Figs. 3j and 7). Intensity scoring was performed on a common four-point scale. Descriptively, 0 represents no staining, 1 represents a low but detectable degree of staining, 2 represents clearly positive staining and 3 represents strong expression. Expression was quantified as an H score, the product of staining intensity multiplied by the percentage of stained cells. Imaging analysis was performed using Aperio ImageScope software (Leica Biosystems).

IHC on mouse tissue. Mice showing late-stage neurological brain tumor symptoms were killed and CNS tissue was collected for histological examination. After 48–72 h in 10% formalin, the brain was cut along the sagittal plane, the spinal cord was transversally cut into 4–6 pieces and then embedded in paraffin and sectioned accordingly for histological evaluation. The location and extent of primary tumor and associated metastases (for medulloblastoma samples only) was analyzed by standard H&E stain. For IHC on mouse tissue sections, the same protocol for TMA analysis was used, but the following primary antibodies and concentrations were utilized: IL-13Ra2 (R&D Systems AF146, 1:400 dilution), HER2 (Sigma HPA001383, 1:500 dilution), EPHA2 (Abcam ab150304, 1:75 dilution) and CD3 (Abcam ab16669, 1:100 dilution). Imaging analysis was performed using Aperio ImageScope software (Leica Biosystems).

Construction, delivery and expression of CAR transgenes. *CAR design, synthesis and cloning.* The HER2-specific scFv FRP5, EPHA2-specific scFv 4H5 and the IL-13Rα2-binding IL-13 mutein used for CAR transgenes were described previously[22,24,25,27,38,54]. The monospecific CAR transgene design consisted of a target-binding domain (FRP5 scFv or 4H5 scFv or IL-13 mutein) connected to a CD28 transmembrane domain followed by the CD28 intracellular signaling domain and a ζ signaling domain of the T cell receptor. The TRI transgene consisted of the three monospecific CAR transgenes targeting IL-13Rα2, HER2 and EPHA2 in tandem separated by 2A viral sequences with restriction enzyme sites at the ends for cloning. All designs were assembled on Clone Manager (Sci-Ed Software) and expression optimized vectors were synthesized by GeneArt Gene Synthesis service (Thermo Fisher Scientific). Synthetic genes were cloned into the Gateway entry vector pDONR 221, sequence-verified, subcloned in frame into an SFG retroviral vector and the construct confirmed using pyro-sequencing (SeqWright DNA-Technology).

Production of retroviral supernatant. To produce retroviral supernatant, human embryonic kidney 293T cells were co-transfected with the CAR transgene-encoding retroviral transfer plasmid, Peg-Pam-e plasmid encoding MoMLV gag-pol and plasmid containing the sequence for RD114 envelope, using GeneJuice (EMD Biosciences). Supernatants containing retroviral vector were collected 48 h and 72 h after transfection.

CAR transgene transduction and T cell expansion. Transduction using retroviral supernatant was performed on anti-CD3 (OKT3)/anti-CD28-activated T cells for genetic modification with the CAR transgene. Briefly, donor peripheral blood mononuclear cells were isolated by Lymphoprep (Bio-One) and activated overnight with OKT3 (Thermo Fisher Scientific) and CD28 monoclonal antibodies (BD Biosciences) at a final concentration of 1 μg ml^{-1}. On day 2, recombinant human IL-7 and IL-15 (PeproTech) were added at a final concentration of 10 ng ml^{-1} and 5 ng ml^{-1}, respectively. On Day 3, cells were collected for retroviral transduction over recombinant fibronectin fragment (Takara-Bio-USA) precoated plates. Subsequently, 2.5×10^5 T cells per well were transduced with retrovirus and expanded after 48–72 h in the presence of 10 ng ml^{-1} IL-7 and 5 ng ml^{-1} IL-15 for 10–15 d before use.

CAR transgene expression on T cells. CAR transgene expression on T cells was detected separately for each molecule using flow cytometry. Cell-surface expression of FRP5 (HER2 CAR) and IL-13 mutein was detected using conjugated Her2.Fc chimeric protein or IL-13Rα2.Fc chimeric protein respectively (R&D Systems) followed by a PE-conjugated goat anti-human Fc (Thermo Fisher Scientific). EPHA2 was detected using EPHA2 tagged with GST (Thermo Fisher Scientific) followed by anti-GST-PE (Abcam). Additionally, FRP5 expression was also detected using AF647 anti-Mouse IgG, F(ab')2 fragment-specific antibody (Jackson ImmunoResearch Laboratories) as required. Flow capture was performed on an Accuri C6 (Becton Dickinson). FlowJo data analysis software (FlowJo) was used for analyses.

Human specimen approval. All human tumor samples were used in accordance with the Research Ethics Board at the Hospital for Sick Children, Toronto, Canada, protocol REB1000024587.

The donor peripheral blood mononuclear cells were derived using the Institutional Review Board-approved protocol H-15280 at Baylor College of Medicine.

Production of lentiviral green fluorescent protein and firefly luciferase supernatant. To produce lentiviral supernatant, human embryonic kidney 293T cells were co-transfected with the pBMN(CMV-copGFP-Luc2-Puro) plasmid, pMD2.G VSVG envelope expressing plasmid and psPAX2 second generation lentiviral packaging plasmid. The supernatants containing the lentiviral particles were collected at 72 h after transfection, centrifuged, filtered, with Lenti-X concentrator added at 1:4 dilution (Clontech, 631231) and titrated for each PDX or cell line for a multiplicity of infection at 0.3 (25%). The plasmid pBMN(CMV-copGFP-Luc2-Puro)[55] was a gift from M. Essand (Addgene plasmid 80389, RRID:Addgene_80389); and pMD2.G and psPAX2 were gifts from D. Trono (Addgene plasmid 12259, RRID:Addgene_12259; and Addgene plasmid 12260, RRID:Addgene_12260).

Patient-derived xenografts and cell lines. *Medulloblastoma.* Med114FH and Med411FH were purchased from the Brain Tumor Resource Laboratory (Olson Lab, Fred Hutchinson Cancer Research Centre). Med114FH derives from a 6-year-old female with an anaplastic large cell medulloblastoma; Med411FH developed from a 3-year-old male with an anaplastic medulloblastoma; MDT-MMB descends from an autopic specimen from a young male with a group 3 high Myc medulloblastoma. Med114FH, Med411FH and MDT-MMB display immunohistochemical and genomic characteristics of group 3 medulloblastoma.

Ependymoma. MDT-PFA4 was derived from a 2-year-old female with PFA ependymoma; MDT-PFA5 was developed from a 1-year-old male presenting with PFA ependymoma; PFA-Ep612 ependymoma cell line[56] (established from a 13-month-old female) was a gift from S. Keir at the Duke Cancer Institute.

To generate stable fluorescent and luminescent lines, PDXs and cell lines were transduced with eGFP-firefly lentiviral particles at a multiplicity of infection of 0.3 (25%). In brief, cells were kept in culture to infect them with protein coding lentiviruses (12 h) in Neurocult NS-A basal medium (human; STEMCELL Technologies, 05750), supplemented with 10 ng ml^{-1} epidermal growth factor (Sigma-Aldrich, E9644), 10 ng ml^{-1} bFGF (STEMCELL Technologies, 02634), 1× B27 (Thermo Fisher Scientific, 17504044), 1× N2 (A1370701), 75 μg ml^{-1} BSA (Gibco, 15260-037), 2 mM l -glutamine (Multicell, 609-065-EL) and 2 μg ml^{-1} heparin (Sigma-Aldrich, H3393). Cellular identities were intermittently confirmed by short tandem repeat genotyping (Geneprint, Promega, B9510) to ensure that it matched the identity of the original patient profile or deposited data.

Orthotopic injection of tumor cells and bioluminescent imaging. Medulloblastoma PDXs (50,000 cells) or ependymoma PDXs (250,000 cells) were stereotactically xenografted in 3 μl total volume into the cerebellum of 6- to 8-week-old NSG immunodeficient mice (Jackson Lab) using the following co-ordinates: 2 mm posterior from Lambda, 1 mm lateral, 3 mm deep and 1 mm retraction to inject at a depth of 2 mm. Xenografted mice were subjected to weekly BLI; mice were given intraperitoneal injections of 150 ng g^{-1} d-luciferin (PerkinElmer, 122796) and anesthetized with 2.5% isoflurane in an induction chamber. Five minutes after injections, mice were imaged using a Xenogen Spectrum (IVIS-200) imaging system and analyzed using Living Image Software (PerkinElmer). Mice received either candidate CAR T cells or non-transduced T cell injection when a baseline bioluminescent tumor signal of 1×10^4 photons per second was reached. Tumors were monitored for regression or progression with BLI and left until neurological symptoms appeared or humane endpoint was reached. Clinical endpoints were assessed and determined by veterinary technicians blinded to experimental groups. Survival of mice was determined using Kaplan–Meier curves and differences evaluated using a log-rank test (Benjamini–Hochberg). Any mice without a brain tumor at endpoint were censored, represented with an 'X' on all associated Kaplan–Meier survival curves, indicating a brain tumor was not the cause of death, correlating with BLI and final H&E analysis. All mouse studies were approved by the Centre for Phenogenomics Animal Care Committee, AUP 21-0100H and our study complies with all relevant ethical regulations.

Mice enrolled as part of the combined preclinical trial therapy began subcutaneous treatment of azacytidine (Celgene) (7 mg m^{-2}, every 3 d × five doses, maximum of six cycles) 1 week after tumor cell engraftment, as described by Kimura et al.[57] and as used in the ongoing clinical trial NCT03206021 (ref. [58]).

Administering CAR T cells. *Lateral ventricle.* Candidate CAR T cells or non-transduced T cells at 5 million cells in 5 μl total volume were stereotactically injected into the LV of mice using the following co-ordinates: 0.5 mm posterior

from Bregma, 1 mm lateral and 3 mm deep. For the second round of therapy, the same co-ordinates and original site of T cell delivery was used.

Intravenous. Mice were heated in their home cage with a heating pad until the dorsal tail vein dilated. To reduce stress a restraining device was used with the tail passed through and held firmly at the tail base. Candidate CAR T cells or non-transduced T cells at 5 million cells in 50 µl total volume were injected into the dorsal tail vein.

Flow cytometry and preparation. PDXs and cell lines were analyzed for EPHA2, HER2 and IL-13Rα2 specific expression pre- and post-azacytidine treatment. Azacytidine was administered at 12 µg ml^{-1} in supplemented Neurocult medium. Cells were analyzed after receiving treatment for 5 d, with a change of medium every 2 d. Control cells received only complete Neurocult medium. Samples were resuspended in PBS-1% BSA for flow cytometry staining. The following antibodies were used for antigen analysis: antibodies IL-13Rα2 (Abcam, ab55275, 1 µg µl^{-1}), anti-HER-2/neu (Becton Dickinson, 340554) and EPHA2 (R&D Systems, MAB3035, 0.25 µg µl^{-1}). Respective control cells were used to set voltages for forward scatter, side scatter and fluorescence. Dead cells were excluded using propidium iodide, SYTOX Blue or DAPI. Flow cytometry data collection was performed using a BD Biosciences LSRII CFI VBYR and analysis was performed using FlowJo (Supplementary Fig. 11).

Statistical analysis. All statistical parameters including the exact value of *n*, type of replicates, the statistical test and significance are reported in all associated figure legends. Data were considered statistically significant when $P<0.05$. A two-sided log-rank Benjamini–Hochberg test was used to calculate survival statistics in three independent PDX models (Figs. 1b, 2b, 3b, 4b and 6b) and two independent PDX models or replicates (Fig. 5b and Supplementary Fig. 13a), with all data represented as minimum of $n=3$ independent animal replicates (exact number defined in all associated figures and legends). A two-sided one-way ANOVA followed by Tukey post hoc test was used to calculate all total flux statistical analysis (Fig. 5c, Extended Data Figs. 3b,c, 8c, 9c and Supplementary Figs. 8c, 9c, 10c and 11c). A two-sided Mann–Whitney *U*-test was used to perform statistical analysis of differentially expressed candidate gene expression across publicly available microarray datasets and candidate target protein expression H score analysis across TMAs (Extended Data Figs. 1a–l, 2a–c,g–i, 3a–c,h–j. A two-sided, unpaired Student's *t*-test was used to calculate all flow cytometry statistics (Supplementary Fig. 14).

Statistics and reproducibility. Extended Data Fig. 1a–c $n=144$ group 3 medulloblastomas, 9 fetal and 6 adult cerebellum independent biological samples. EPHA2: group 3 medulloblastoma versus adult normal cerebellum, $P=0.00018$; group 3 medulloblastoma versus fetal normal cerebellum, $P=0.018$. HER2: group 3 medulloblastoma versus adult normal cerebellum, $P=0.01$; group 3 medulloblastoma versus fetal normal cerebellum, $P=0.01$. IL-13Rα2: group 3 medulloblastoma versus adult normal cerebellum, $P=0.7$; group 3 medulloblastoma versus fetal normal cerebellum, $P=0.00001$.

Extended Data Fig. 1d–f $n=67$ group 3α medulloblastomas, 37 group 3β medulloblastomas, 40 group 3γ medulloblastomas, 9 fetal and 6 adult cerebellum independent biological samples. EPHA2: group 3α versus adult normal cerebellum, $P=0.0001$; group 3α versus normal fetal cerebellum, $P=0.0001$; group 3β versus adult normal cerebellum, $P=0.0003$; group 3β versus normal fetal cerebellum, $P=0.0003$; group 3γ versus adult normal cerebellum, $P=0.0003$; group 3γ versus normal fetal cerebellum, $P=0.0003$. HER2: group 3α versus adult normal cerebellum, $P=0.000042$; group 3α versus normal fetal cerebellum, $P=0.06$; group 3β versus adult normal cerebellum, $P=0.03$; group 3β versus normal fetal cerebellum, $P=0.0001$; group 3γ versus adult normal cerebellum, $P=0.007$; group 3γ versus normal fetal cerebellum, $P=0.01$. IL-13Rα2: group 3α versus adult normal cerebellum, $P=0.096$; group 3α versus normal fetal cerebellum, $P=0.0001$; group 3β versus adult normal cerebellum, $P=0.21$; group 3β versus normal fetal cerebellum, $P=0.17$; group 3γ versus adult normal cerebellum, $P=0.134$; group 3γ versus normal fetal cerebellum, $P=0.0001$.

Extended Data Fig. 1g–i $n=70$ WNT medulloblastomas, 223 SHH medulloblastomas, 326 group 4 medulloblastomas, 9 normal fetal and 6 normal adult cerebellum independent biological samples. EPHA2: WNT medulloblastoma versus adult normal cerebellum, $P=0.0001$; WNT medulloblastoma versus fetal normal cerebellum, $P=0.0283$; SHH medulloblastoma versus adult normal cerebellum, $P=0.0191$; SHH medulloblastoma versus fetal normal cerebellum, $P=0.2$; group 4 medulloblastoma versus adult normal cerebellum, $P=0.0191$; group 4 medulloblastoma versus fetal normal cerebellum, $P=0.2$. HER2: WNT medulloblastoma versus adult normal cerebellum, $P=0.0001$; WNT medulloblastoma versus fetal normal cerebellum, $P=0.5$; SHH medulloblastoma versus adult normal cerebellum, $P=0.5$; SHH medulloblastoma versus fetal normal cerebellum, $P=0.0003$; group 4 medulloblastoma versus adult normal cerebellum, $P=0.0001$; group 4 medulloblastoma versus fetal normal cerebellum, $P=0.0063$. IL-13Rα2: WNT medulloblastoma versus adult normal cerebellum, $P=0.5$; WNT medulloblastoma versus fetal normal cerebellum, $P=0.0001$; SHH medulloblastoma versus adult normal cerebellum, $P=0.65$; SHH medulloblastoma versus fetal normal cerebellum, $P=0.0001$; group 4 medulloblastoma versus adult normal cerebellum, $P=0.06$; group 4 medulloblastoma versus fetal normal cerebellum, $P=0.2$.

Extended Data Fig. 1j–l $n=11$ EPHA2, 11 HER2 and 12 IL-13Rα2 group 3 biological samples, representing one technical replicate.

Supplementary Fig. 5a MDT-PFA4 with 2.5×10^6 CARs or T cells: 24 h: TRI versus T cells, $P=0.006$; TRI versus HER2, $P=0.007$; T cells versus HER2, $P=0.9867$. 48 h: TRI versus T cells $P=0.0005$; TRI versus HER2, $P=0.0024$; T cells versus HER2, $P=0.3302$. 72 h: TRI versus T cells, $P=0.0011$; TRI versus HER2 $P=0.0121$; T cells versus HER2, $P=0.0985$. 96 h: TRI versus T cells, $P=0.0004$; TRI versus HER2, $P=0.0111$; T cells versus HER2, $P=0.0301$. 120 h: TRI versus T cells, $P=0.0027$, TRI versus HER2, $P=0.0771$; T cells versus HER2, $P=0.0469$. MDT-PFA4 with 5.0×10^6 CARs or T cells: 24 h: TRI versus T cells, $P=0.00001$; TRI versus HER2, $P=0.0006$; T cells versus HER2, $P=0.0852$. 48 h: TRI versus T cells, $P=0.00001$; TRI versus HER2, $P=0.0059$; T cells versus HER2, $P=0.0069$. 72 h: TRI versus T cells, $P=0.001$; TRI versus HER2, $P=0.1831$; T cells versus HER2, $P=0.0071$. 96 h: TRI versus T cells, $P=0.008$; TRI versus HER2, $P=0.553$; T cells versus HER2, $P=0.0265$. 120 h: TRI versus T cells, $P=0.0244$; TRI versus HER2, $P=0.7381$; T cells versus HER2, $P=0.0612$. MDT-PFA4 with 10×10^6 CARs or T cells: 24 h: TRI versus T cells, $P=0.0007$; TRI versus HER2, $P=0.0009$; T cells versus HER2, $P=0.9874$. 48 h: TRI versus T cells, $P=0.00001$; TRI versus HER2, $P=0.0017$; T cells versus HER2, $P=0.0262$. 72 h: TRI versus T cells, $P=0.00001$; TRI versus HER2, $P=0.0012$; T cells versus HER2, $P=0.0005$. 96 h: TRI versus T cells $P=0.00001$; TRI versus HER2, $P=0.0066$; T cells versus HER2, $P=0.00001$. 120 h: TRI versus T cells, $P=0.00001$; TRI versus HER2, $P=0.0266$; T cells versus HER2, $P=0.0001$. MDT-PFA5 with 2.5×10^6 CARs or T cells: 24 h: T cells versus HER2, $P=0.05$. 48 h: TRI versus T cells, $P=0.891$; TRI versus HER2, $P=0.1602$; T cells versus HER2, $P=0.088$. 72 h: TRI versus T cells, $P=0.1262$; TRI versus HER2, $P=0.0623$, T cells versus HER2, $P=0.847$. 96 h: TRI versus T cells, $P=0.0184$; TRI versus HER2, $P=0.0543$; T cells versus HER2, $P=0.6507$. 120 h: TRI versus T cells, $P=0.0083$; TRI versus HER2, $P=0.0332$; T cells versus HER2, $P=0.4703$. MDT-PFA5 with 5.0×10^6 CARs or T cells: 24 h: TRI versus T cells, $P=0.0267$; TRI versus HER2, $P=0.9923$; T cells versus HER2, $P=0.0309$. 48 h: TRI versus T cells, $P=0.0024$; TRI versus HER2, $P=0.9921$; T cells versus HER2, $P=0.0027$. 72 h: TRI versus T cells, $P=0.00001$; TRI versus HER2, $P=0.9932$; T cells versus HER2, $P=0.00001$. 96 h: TRI versus T cells, $P=0.00001$; TRI versus HER2, $P=0.9979$; T cells versus HER2, $P=0.0001$. 120 h: TRI versus T cells, $P=0.0001$; TRI versus HER2, $P=0.9134$; T cells versus HER2, $P=0.0001$. MDT-PFA5 with 10×10^6 CARs or T cells: 24 h: TRI versus T cells, $P=0.2971$; TRI versus HER2, $P=0.2798$; T cells versus HER2, $P=0.9987$. 48 h: TRI versus T cells, $P=0.0383$; TRI versus HER2, $P=0.2741$; T cells versus HER2, $P=0.3274$. 72 h: TRI versus T cells, $P=0.029$; TRI versus HER2, $P=0.6489$; T cells versus HER2, $P=0.0896$. 96 h: TRI versus T cells, $P=0.0479$; TRI versus HER2, $P=0.9927$; T cells versus HER2, $P=0.0557$. 120 h: TRI versus T cells, $P=0.2777$; TRI versus HER2, $P=0.6098$; T cells versus HER2, $P=0.0796$.

Supplementary Fig. 8c Infusion of 2.5×10^6 non-transduced T cells: day 0 i.v. versus LV, $P=0.115$; day 30 i.v. versus LV, $P=0.05$. Infusion of 5.0×10^6 non-transduced T cells: day 0 i.v. versus LV, $P=0.814$; day 30 i.v. versus LV, $P=0.988$. Infusion of 10×10^6 non-transduced T cells: day 0 i.v. versus LV, $P=0.796$; day 30 i.v. versus LV, $P=0.114$.

Supplementary Fig. 9c Infusion of 2.5×10^6 non-transduced T cells: day 0 i.v. versus LV, $P=0.967$; day 30 i.v. versus LV, $P=0.006$. Infusion of 5.0×10^6 non-transduced T cells: day 0 i.v. versus LV, $P=0.06$; day 30 i.v. versus LV, $P=0.05$. Infusion of 10×10^6 non-transduced T cells: day 0 i.v. versus LV, $P=0.67$; day 30 i.v. versus LV, $P=0.0387$.

Supplementary Fig. 10c Infusion of 2.5×10^6 TRI CAR T cells: day 0 i.v. versus LV, $P=0.341$; day 30 i.v. versus LV, $P=0.0539$. Infusion of 5.0×10^6 TRI CAR T cells: day 0 i.v. versus LV, $P=0.324$; day 30 i.v. versus LV, $P=0.894$. Infusion of 10×10^6 TRI CAR T cells: day 0 i.v. versus LV, $P=0.52$; day 30 i.v. versus LV, $P=0.934$.

Supplementary Fig. 11c Infusion of 2.5×10^6 TRI CAR T cells: day 0 i.v. versus LV, $P=0.357$; day 30 i.v. versus LV, $P=0.153$. Infusion of 5.0×10^6 TRI CAR T cells: day 0 i.v. versus LV, $P=0.515$; day 30 i.v. versus LV, $P=0.177$. Infusion of 10×10^6 TRI CAR T cells: day 0 i.v. versus LV, $P=0.94$.

Microarray data, analysis and availability. Differential gene expression analysis between the primary and metastatic medulloblastoma samples was performed on a cohort of 12 paired primary metastatic tumors collected in the MAGIC consortium and profiled using DNA methylation analysis as previously described[59]. In brief, DNA methylation was generated using the Illumina Infinium HumanMethylation450 BeadChip array (450k array). Samples were normalized using the SWAN as part of the R/Bioconductor minfi package (v.1.12.0). The accession number for the medulloblastoma primary metastatic paired Affymetrix Array Data used in this paper, generated by Wang et al.[59] is GEO: GSE63670.

Differential gene expression analysis of primary medulloblastoma samples as subgroups and associated subtypes was performed on a cohort of 763 primary medulloblastoma samples, compiled by the MAGIC consortium and analyzed using genome-wide methylation and expression profiles, as previously described[9]. In brief, to generate gene expression profiling, the Affymetrix Gene

1.1 ST array was used; all samples were analyzed on the Illumina Infinium HumanMethylation450 BeadChip. The accession number for the primary medulloblastoma methylation data used in this paper, generated by Cavalli et al.[9] is GEO: GSE85218.

Differential gene expression analysis of primary ependymoma samples was performed using gene expression profiles from a cohort of 100 ependymomas generated using the Affymetrix Exon 1.0 ST Gene Chip array, as previously described[31]. In brief, arrays were quantile normalized (sketch) and summarized using PLIER and PM-GCBG background correction. Probe sets were annotated according to the human genome build HG19 (GRCh37). Gene expression and aCGH data for this dataset can be found at GEO: GSE27279.

Cell culture assays. For in vitro co-culture and dose–response assays, ependymomas MDT-PFA4 and MDT-PFA5 were used at a plate density of 1×10^4 cells per well of a precoated laminin and poly-l -lysine 96-well plate in a medium mixture (1:1 ratio) of complete Neurocult medium to Dulbecco's Modified Eagle's Medium and Clicks medium (1:1 ratio) plus 10% fetal calf serum. Triplicate wells were plated for each condition. After 24 h, appropriate controls or CAR T cells were added in a ratio of 1:10, 1:20 or 1:40 T cells to tumor cells. Phase confluency analysis was conducted using an Incucyte Zoom over a 120-h time course. Analysis was performed following confluency normalization to hour set at 0 for all replicates and conditions.

For cytokine production analysis, 3×10^5 tumor cells were co-cultured for 24 h at a 1:20 ratio with non-transduced T cells or CAR T cells. Duplicate wells were plated for each condition. Culture supernatants were collected and analyzed for interferon-γ and IL-2 by ELISA (R&D Systems).

Reporting Summary. Experimental summaries can also be found within the Nature Research Reporting Summary.

Data availability

All requests for raw and analyzed data and materials are promptly reviewed by the Hospital for Sick Children to verify whether the request is subject to any intellectual property or confidentiality obligations. Any materials that can be shared will be released via a material transfer agreement. All raw and analyzed sequencing datasets analyzed during the current study are open source, referenced and available from the following repositories: primary metastasis medulloblastoma pairs DNA methylation analysis, GSE63670; primary medulloblastoma genome-wide methylation and expression profile analysis, GSE85218; and primary ependymoma Affymetrix chip array analysis, GSE27279. All CAR T cell constructs used within the study have been previously published.

References

54. Azemar, M. et al. Regression of cutaneous tumor lesions in patients intratumorally injected with recombinant single-chain antibody-toxic targeted to ErbB2/HER2. *Breast Cancer Res. Treat.* **82**, 155–164 (2003).
55. Jin, C. et al. Safe engineering of CAR T cells for adoptive cell therapy of cancer using long-term episomal gene transfer. *EMBO Mol. Med.* **8**, 702–711 (2016).
56. McLendon, R. E. et al. Production and characterization of two ependymoma xenografts. *J. Neuropathol. Exp. Neurol.* **55**, 540–548 (1996).
57. Kimura, S. et al. Antiproliferative and antitumor effects of azacytidine against the human myelodysplastic syndrome cell line SKM-1. *Anticancer Res.* **32**, 795–798 (2012).
58. Ramaswamy, V. Treatment of children with refractory brain/solid tumors and recurrent ependymoma. ClinicalTrials.gov Identifier: NCT03206021 (2017).
59. Wang, X. et al. Medulloblastoma subgroups remain stable across primary and metastatic compartments. *Acta Neuropathol.* **154**, 2262–2265 (2014).

Acknowledgements

M.D.T. is supported by the National Institutes of Health (R01CA148699 and R01CA159859), the Pediatric Brain Tumour Foundation, the Terry Fox Research Institute, the Canadian Institutes of Health Research, the Cure Search Foundation, b.r.a.i.n.child, Meagan's Walk, SWIFTY Foundation, the Brain Tumour Charity, Genome Canada, Genome BC, Genome Quebec, the Ontario Research Fund, Worldwide Cancer Research, V-Foundation for Cancer Research and the Ontario Institute for Cancer Research through funding provided by the Government of Ontario. M.D.T. is also supported by a Canadian Cancer Society Research Institute Impact grant, a Cancer Research UK Brain Tumour Award and by a Stand Up To Cancer (SU2C) St. Baldrick's Pediatric Dream Team Translational Research Grant (SU2C-AACR-DT1113) and SU2C Canada Cancer Stem Cell Dream Team Research Funding (SU2C-AACR-DT-19-15) provided by the Government of Canada through Genome Canada and the Canadian Institutes of Health Research, with supplementary support from the Ontario Institute for Cancer Research through funding provided by the Government of Ontario. SU2C is a program of the Entertainment Industry Foundation administered by the American Association for Cancer Research. M.D.T. is also supported by the Garron Family Chair in Childhood Cancer Research at the Hospital for Sick Children and the University of Toronto. N.A. is supported by National Institutes of Health (U54 CA232568-01), SU2C St. Baldrick's Pediatric Dream Team Translational Research Grant (SU2C-AACR-DT1113). L.K.D. was supported by funding from Brain Canada NeuroDevNet. We thank P. Rose Matthew for her valuable help in making CAR T cells; S. Gottschalk for designing and constructing EPHA2 CAR; D. Trono for gifting psPAX2 and pMD2.G plasmids; S. Keir and D. Bigner for gifting Ep612 cells; and M. Essand for gifting pBMN(CMV-copGFP-Luc2-Puro) plasmid. The authors thank J. Loukides (Manager, Brain Tumour Biobank at SickKids) and recognize the Labatt Brain Tumour Research Centre and the Michael and Amira Dan Brain Tumour Bank Network. We gratefully thank the Pathology Research Program Laboratory, UHN, for their pathology assistance and the Centre for Phenogenomics for their animal husbandry support and BLI assistance. We thank S. Archer for technical writing assistance and editing and A. Carlow for manuscript support.

Author contributions

L.K.D. designed, performed and analyzed the majority of experiments in this study and co-wrote the manuscript. A.D. performed and analyzed IHC. K.B., S.K.J., K.F., M.H. and A.Z.G. designed CAR constructs, produced CAR T cells and presented technical assistance. D.S. assisted with sample collections, DNA extractions, statistical analysis and figure preparation. R.V.O., Z.A. and S.V. supported azacytidine analysis. D.P. and C.R. provided in vitro support. B.L.H. and L.G. aided with MB PDX expansions and offered technical support. A.M., J.G.P., T.D. and B.L. assisted with animal husbandry, necropsies and drug administrations. J.H, A.G.S. and P.D.A. assisted with LV infusions. A.S.M., F.M.G.C. and V.R. helped perform microarray analysis. S.C.M. performed microarray and methylation analysis. C.N. and C.M.K.-F. aided with sample collection and drug administration. M.L.B. performed computational CAR modeling. M.C.V. assisted with BLI. A.M. and S.A.K. helped with EP cell expansions. L.Q. and N.H. provided pathology support. X.W. provided technical and reagents assistance. R.S. provided technical assistance. C.D., A.C.M.J., A.R., L.H., M.L., P.B. and K.K. supported manuscript and figure preparation. O.S. performed imaging analysis. C.C.F. provided histology samples. S.Y. and J.H. provided the multicenter EP TMA. C.H. provided the SickKids MB TMA. K.A. supplied sequencing assistance and support. M.D. provided pathology analysis. J.M.M. provided CHOP MB TMA and provided technical support. P.H.S. provided valuable pathology support. N.A. and M.D.T. supervised the project and co-wrote the manuscript.

Competing interests

The authors declare no competing interests.

Additional information

Extended data is available for this paper at https://doi.org/10.1038/s41591-020-0827-2.

Supplementary information is available for this paper at https://doi.org/10.1038/s41591-020-0827-2.

Correspondence and requests for materials should be addressed to M.D.T.

Peer review information Saheli Sadanand was the primary editor on this article and managed its editorial process and peer review in collaboration with the rest of the editorial team.

Reprints and permissions information is available at www.nature.com/reprints.

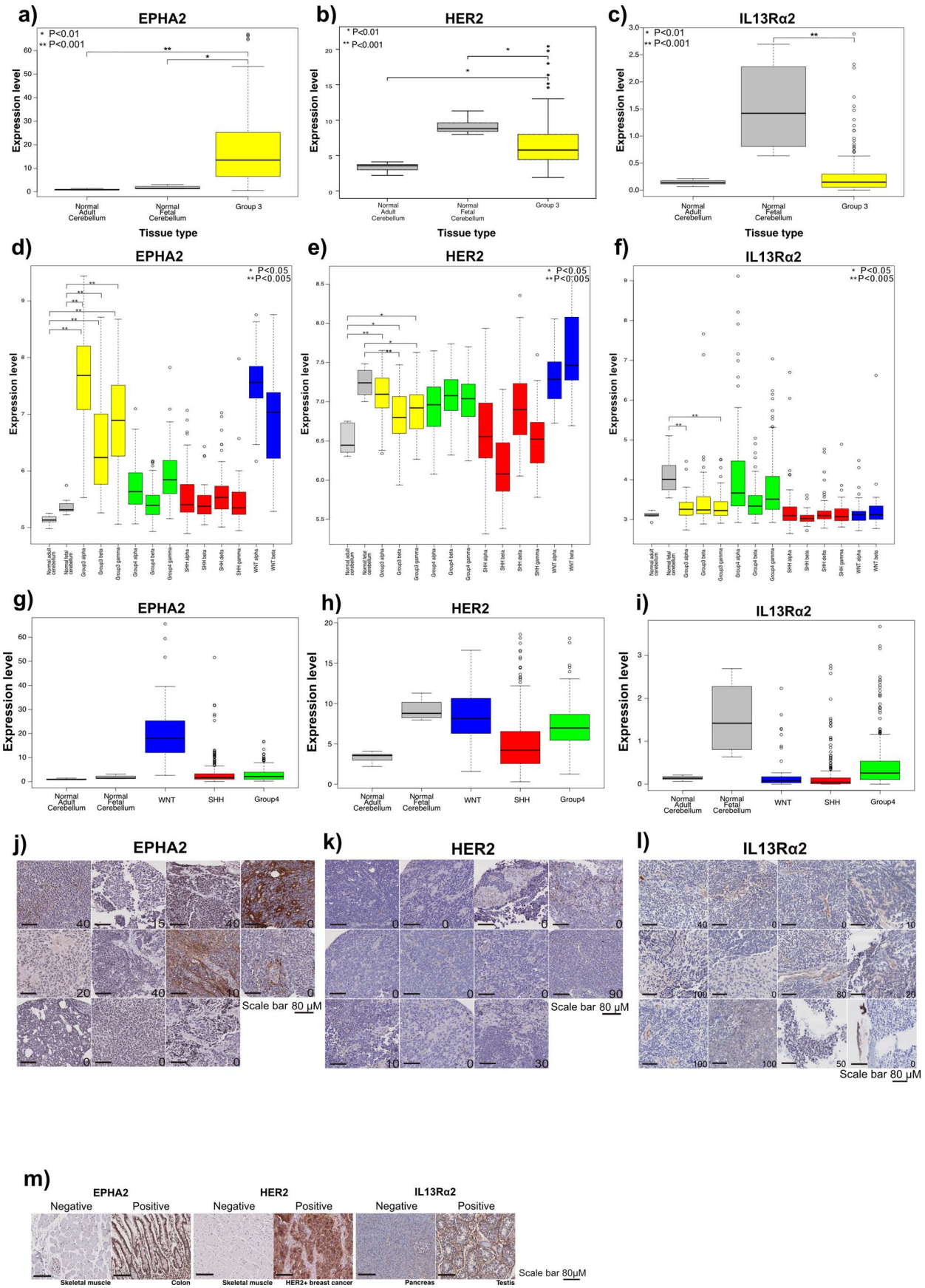

Extended Data Fig. 1 | See next page for caption.

Extended Data Fig. 1 | EPHA2, HER2 and IL13Rα2 are immunotherapy targets in Group 3 medulloblastoma. a, EPHA2 mRNA expression in human Group 3 medulloblastoma versus normal human adult and fetal cerebellum; **b**, HER2 expression in human Group 3 medulloblastoma versus normal human adult and fetal cerebellum; and **c**, IL13Rα2 expression in human Group 3 medulloblastoma versus normal human fetal and adult cerebellum, by expression microarray, two-sided Mann-Whitney U test. mRNA differential expression across human medulloblastoma subtypes versus normal adult and fetal cerebellum control for **d**, EPHA2; **e**, HER2; and **f**, IL13Rα2; as compared by expression microarray, * $P < 0.05$; ** $P < 0.005$, two-sided Mann-Whitney U-test. **g**, EPHA2 mRNA expression in human WNT, SHH and Group 4 medulloblastoma subgroups versus normal human adult and fetal cerebellum **h**, HER2 mRNA expression in human WNT, SHH and Group 4 medulloblastoma subgroups versus normal human adult and fetal cerebellum; and **i**. IL13Rα2 mRNA expression in human WNT, SHH and Group 4 medulloblastoma subgroups versus normal human adult and fetal cerebellum as compared by expression microarray, two-sided one-way ANOVA with post-hoc Tukey HSD. All boxplot center lines show data median; box limits indicate the 25th and 75th percentiles; lower and upper whiskers extend 1.5 times the interquartile range (IQR) from the 25th and 75th percentiles, respectively. Outliers are represented by individual points. Error bars ± SEM **j**, H score of EPHA2 IHC ($P = 0.6$); **k**, H score of HER2 IHC ($P = 0.6$); **l**, H score of IL13Rα2 IHC ($P = 0.9$ two-sided Mann-Whitney U test) in human paediatric primary and metastases or recurrence for Group 3 medulloblastoma. **m**, Normal skeletal muscle used for EPHA2 and HER2-negative controls; normal colon used for EPHA2-positive controls; HER2-positive breast cancer used as HER2-positive controls; normal pancreas and testis used for IL13Rα2-negative and positive controls, respectively. Scale bar represents 100 mM, data represents 3 Biological replicates.

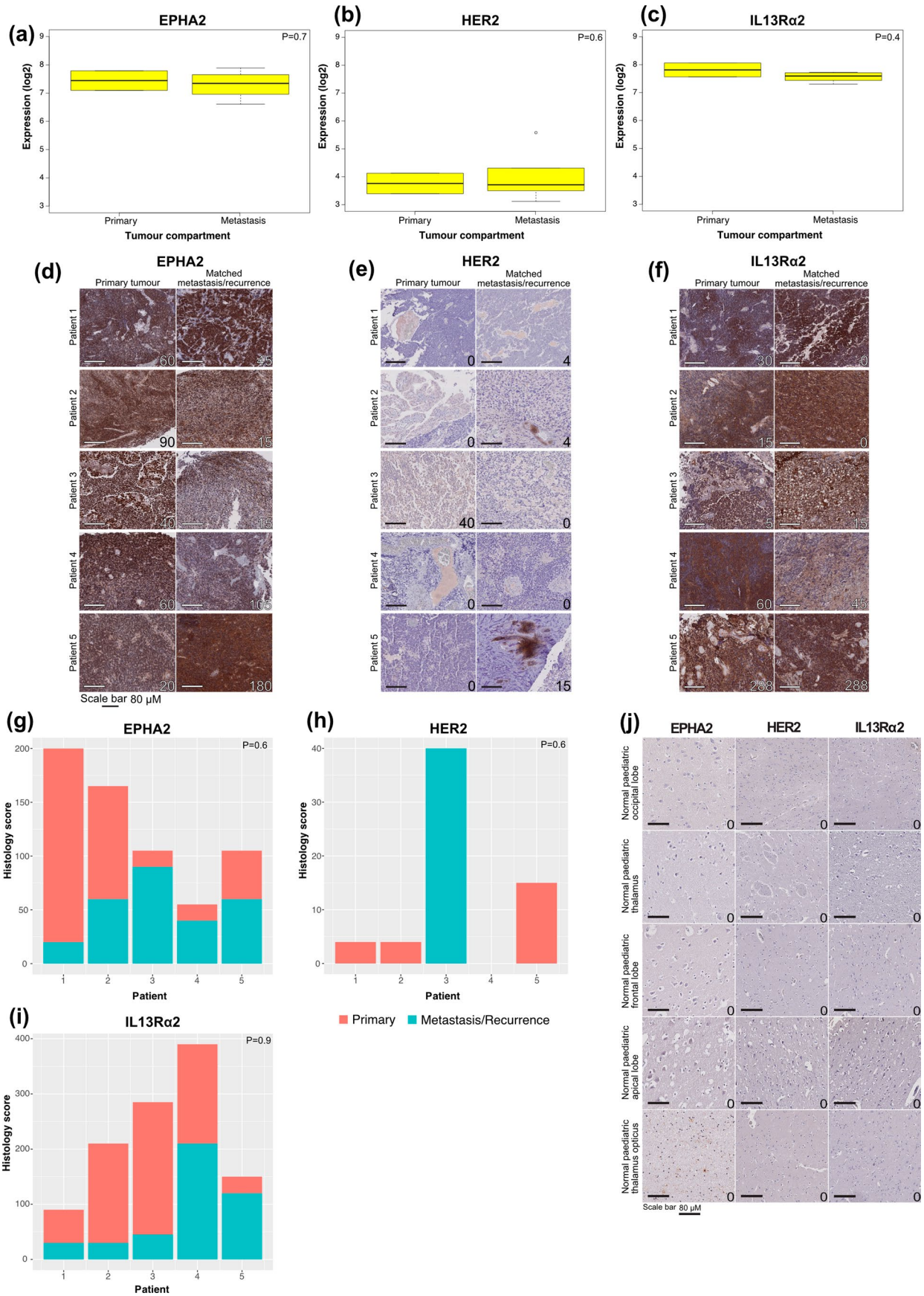

Extended Data Fig. 2 | See next page for caption.

Extended Data Fig. 2 | Defining EPHA2, HER2 and IL13Rα2 as immunotherapy targets in Group 3 primary and matched metastases or recurrence. **a**, EPHA2 expression in human primary and metastatic Group 3 medulloblastomas; **b**, HER2 expression in human primary and metastatic Group 3 medulloblastoma; and **c**, IL13Rα2 is expressed in both human primary and metastatic compartments of Group 3 medulloblastoma, by expression microarray, n = 2 primary and 6 metastatic or recurrence group 3 medulloblastomas. All boxplot center lines show data median; box limits indicate the 25th and 75th percentiles; lower and upper whiskers extend 1.5 times the interquartile range (IQR) from the 25th and 75th percentiles, respectively. Outliers are represented by individual points. **d**, EPHA2 immunohistochemistry (IHC); **e**, HER2 IHC; and **f**, IL13Rα2 IHC staining analysis of paired human paediatric primary and metastases or recurrence in Group 3 medulloblastoma, representative membrane-staining H-scores displayed in lower corner. Scale bars represent 80 μM, data represents 3 biological replicates. **g**, H score of EPHA2 IHC ($P = 0.6$ two-sided Mann-Whitney U test); **h**, H score of HER2 IHC ($P = 0.6$ two-sided Mann-Whitney U test); **i**, H score of IL13Rα2 IHC ($P = 0.9$ two-sided Mann-Whitney U test) in n = 6 independent human paediatric primary and metastases or recurrence for Group 3 medulloblastoma samples; **j**, EPHA2, HER2 and IL13Rα2 protein expression in normal paediatric brain compartments. Scale bar represents 80 μM, numbers represent H-scores data represents 6 biological replicates.

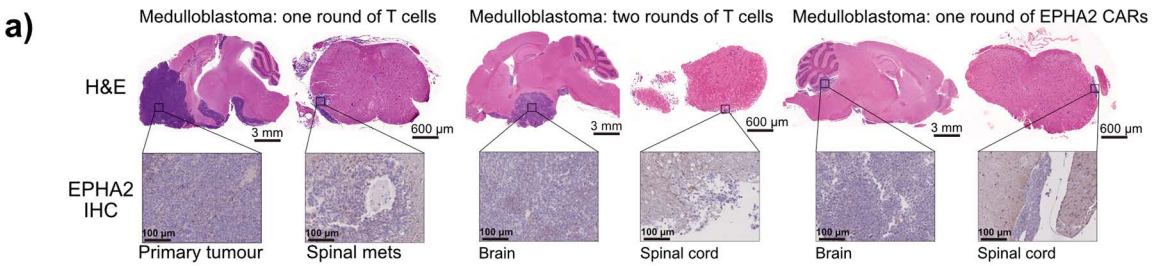

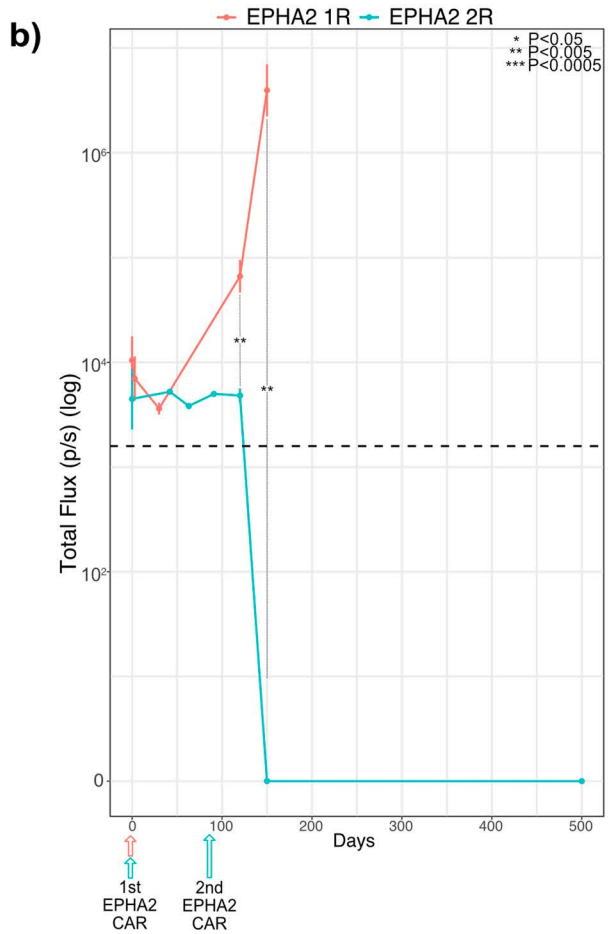

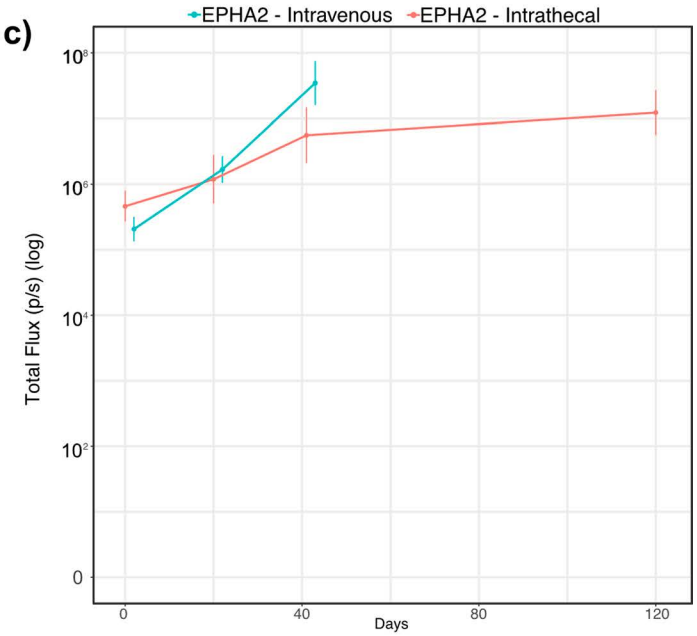

Extended Data Fig. 3 | Two doses of EPHA2-CAR T cells improves antitumour response in Group 3 medulloblastoma orthotopic xenograft models. **a**, Hematoxylin-eosin (H&E) staining analysis of NSG mice xenografted with luciferase-expressing MDT-MMB, following one round of EPHA2 CAR T-cells and one versus two rounds of non-transduced T-cells, with associated IHC analysis for EPHA2 protein expression for the cerebellar tumour and matched spinal metastases, data represents 3 independent replicates. **b**, Measurement log Total Flux (photon/second) following one versus two rounds of intraventricular EPHA2 CAR T-cell therapy. ***P < 0.0005, **P < 0.005, *P < 0.05 by two-sided ANOVA followed by Tukey post hoc test, n = 5 MDT-MMB treated with EPHA2 CAR T-cells 1 round of therapy, n = 3 MDT-MMB treated with EPHA2 CAR T-cells 2 rounds of therapy, error bars represent SEM, centre line represents the mean. EPHA2 one round versus EPHA2 two rounds: Day 1: P = 0.3796; Day 120: P = 0.0009112; Day 150 P = 0.00141. **c**, Measurement of log Total Flux (photon/second) following one round of intraventricular versus i.v. EPHA2 CAR T-cell therapy. ***P < 0.0005, **P < 0.005, *P < 0.05, by two-sided ANOVA followed by Tukey post hoc test, n = 19 EPHA2 CAR T-cells delivered intraventricularly, n = 15 EPHA2 CAR T-cells delivered IV, error bars represent SEM, centre line represents mean. EPHA2 IV versus EPHA2 intraventricular: Day 1: P = 0.2038; Day 21: P = 0.2321; Day 42 P = 0.2731.

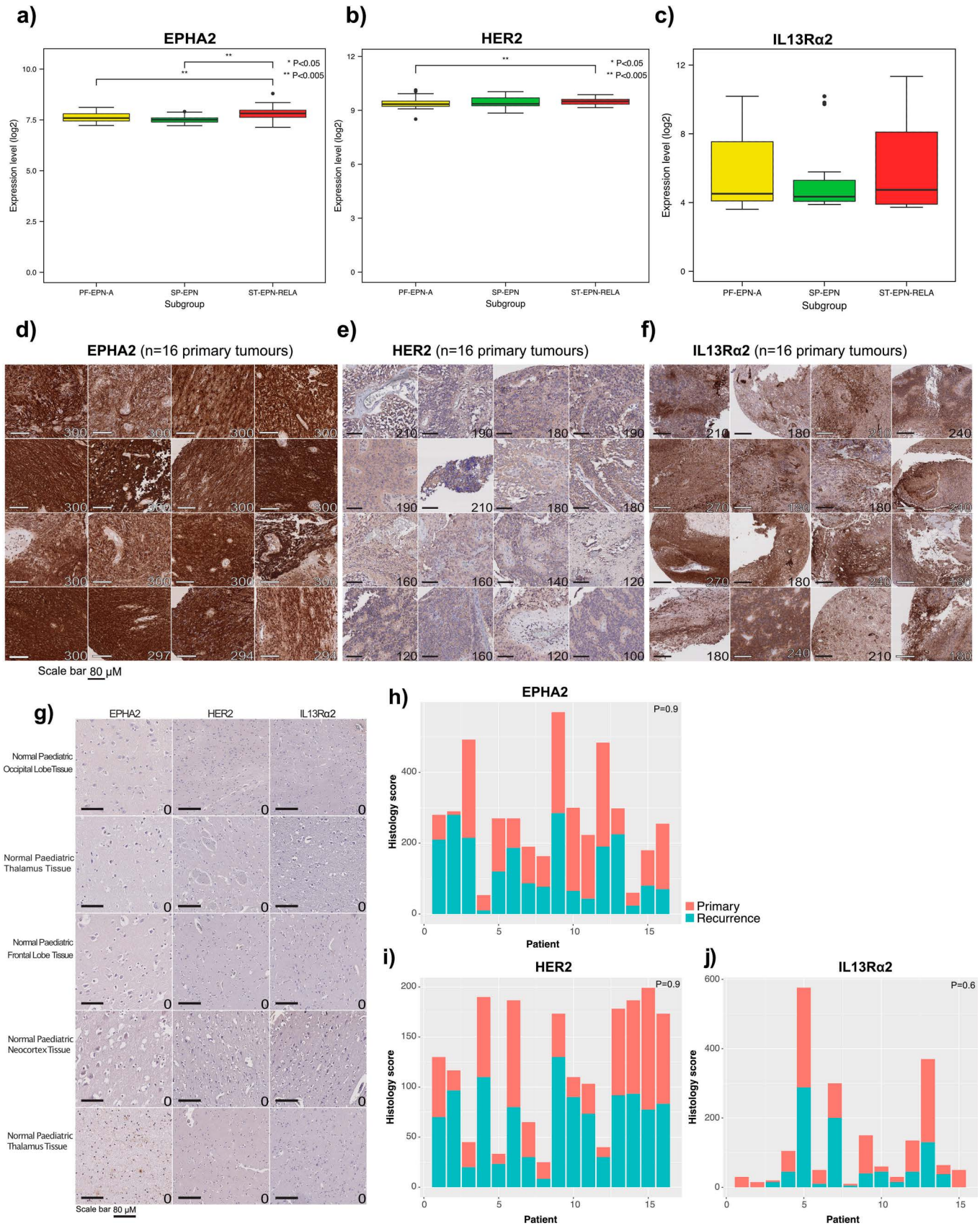

Extended Data Fig. 4 | See next page for caption.

Extended Data Fig. 4 | EPHA2, HER2 and IL13Rα2 are immunotherapy targets in PFA ependymoma. a, EPHA2 differential expression across ependymoma subgroups (PF-EPN-A vs ST-EPN-RELA P = 0.05; PF-EPN-A vs SP-EPN P = 0.5207, two-sided Mann Whitney U test); **b**, HER2 differential expression across ependymoma subgroups (PF-EPN-A vs ST-EPN-RELA P = 0.0026; PF-EPN-A vs SP-EPN P = 0.146; SP-EPN vs ST-EPN-RELA P = 0.0027, two-sided Mann Whitney U test); and **c**, IL13Rα2 differential expression across ependymoma subgroups (PF-EPN-A vs ST-EPN-RELA P = 0.99; PF-EPN-A vs SP-EPN P = 0.7024, two-sided Mann Whitney U test), as compared by expression microarray, n = 54 PF-EPN-A, 15 SP-EPN, 31 ST-EPN-RELA. All boxplot centre lines show data median; box limits indicate the 25th and 75th percentiles; lower and upper whiskers extend 1.5 times the interquartile range (IQR) from the 25th and 75th percentiles, respectively. Outliers are represented by individual points. **d**, IHC membrane staining of EPHA2 in ependymoma primary tumour TMAs; **e**, IHC membrane staining of HER2 in ependymoma primary tumour TMAs; and **f**, IHC membrane staining of IL13Rα2 in ependymoma primary tumour TMAs, representative membrane-staining H-scores displayed in lower corner. Scale bars represent 80 μM. **g**, EPHA2, HER2 and IL13Rα2 protein expression in normal paediatric brain compartments, as comparative protein staining analysis in the normal brain. Scale bar represents 80 μM, numbers represent H-scores, data representative of 2 independent replicates. **h**, Summary of membrane-staining H score of EPHA2 IHC of human paediatric paired primary and recurrence for PFA ependymoma (P = 0.9 two-sided Mann-Whitney U test) **i**, Summary of membrane-staining H score of HER2 IHC of human paediatric paired primary and recurrence for PFA ependymoma (P = 0.9 two-sided Mann-Whitney U test) **j**, Summary of membrane-staining H score of IL13Rα2 IHC of human paediatric paired primary and recurrence for PFA ependymoma (P = 0.6 two-sided Mann-Whitney U test), n = 16 primary and 16 matched recurrences of biologically independent paired samples.

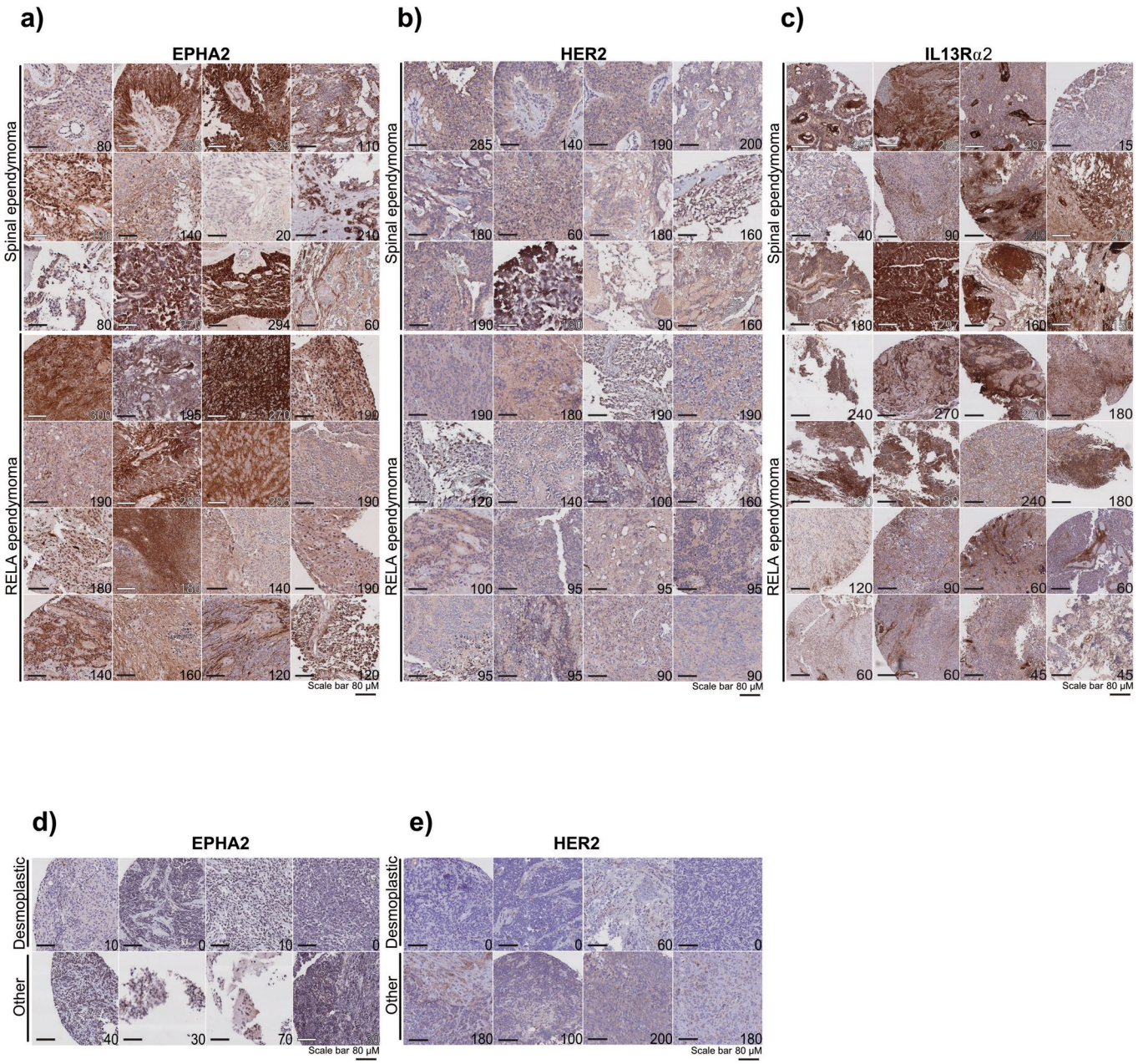

Extended Data Fig. 5 | EPHA2 protein expression in primary paediatric ependymoma. a, EPHA2 protein expression in primary paediatric ependymoma. Top panel displays spinal ependymoma, bottom panel displays RELA ependymoma. **b**, HER2 protein expression in primary paediatric ependymoma. Top panel displays spinal ependymoma, bottom panel displays RELA ependymoma. **c**, IL13Rα2 protein expression in primary paediatric ependymoma. Top panel displays spinal ependymoma, bottom panel displays RELA ependymoma. **d**, EPHA2 protein expression in primary paediatric, desmoplastic medulloblastoma by CHOP TMA. **e**, HER2 protein expression in primary paediatric, desmoplastic medulloblastoma by CHOP TMA. Scale bar represents 80 μM. Data representative of 3 biological replicates.

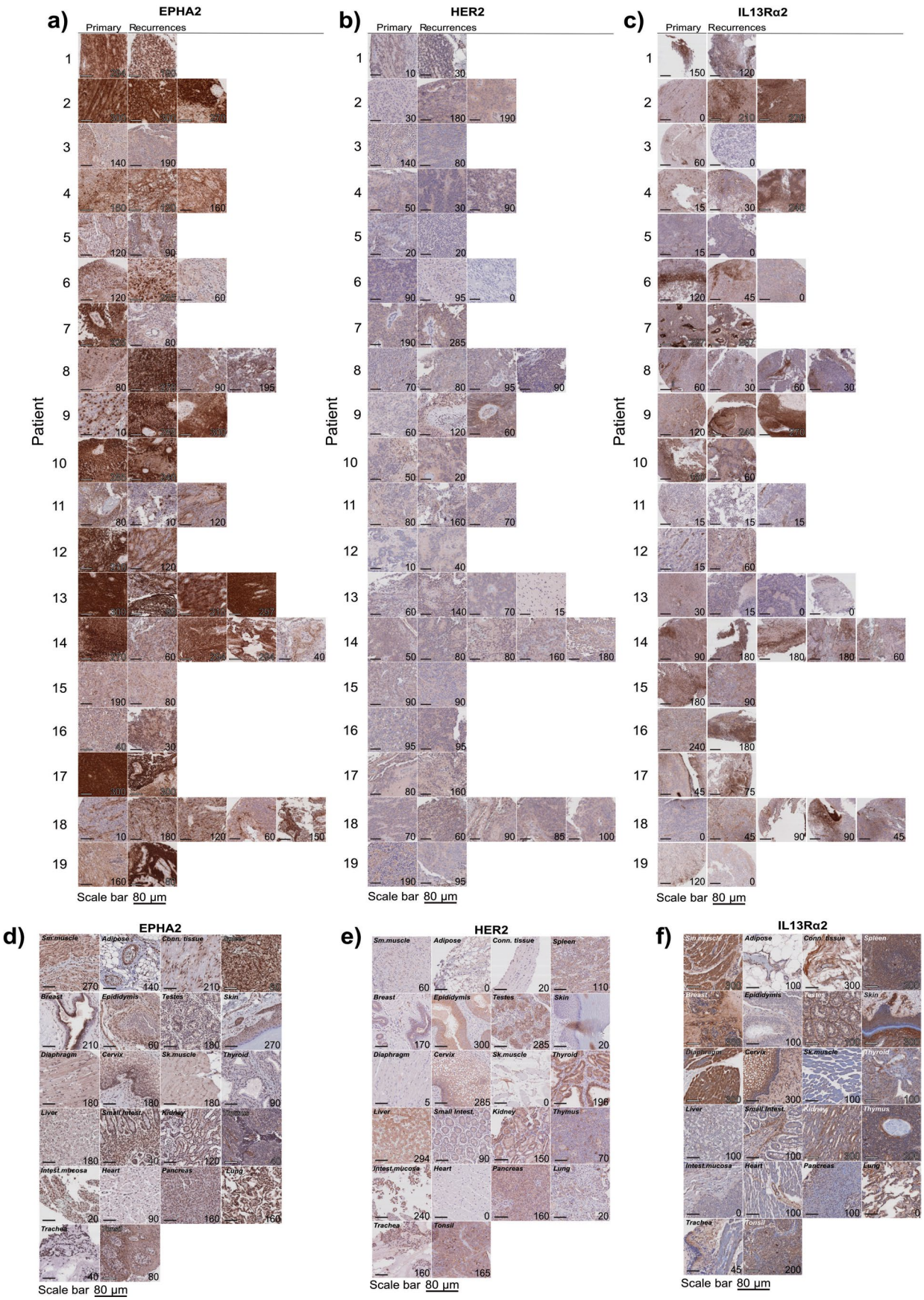

Extended Data Fig. 6 | See next page for caption.

Extended Data Fig. 6 | EPHA2 protein expression in primary paediatric ependymoma and matched recurrences. a, EPHA2 protein expression in primary paediatric ependymoma and matched recurrences. **b**, HER2 protein expression in primary paediatric ependymoma and matched recurrences. **c**, IL13Rα2 protein expression in primary paediatric ependymoma and matched recurrences. **d**, EPHA2 protein expression in primary paediatric medulloblastoma. Top panel displays SHH medulloblastoma, bottom panel displays Group 4 medulloblastoma. **e**, HER2 protein expression in primary paediatric medulloblastoma. Top panel displays SHH medulloblastoma, bottom panel displays Group 4 medulloblastoma. **f**, IL13Rα2 protein expression in primary paediatric medulloblastoma. Top panel displays SHH medulloblastoma, bottom panel displays Group 4 medulloblastoma. Scale bar represents 80 μM. Data represents 3 biological replicates.

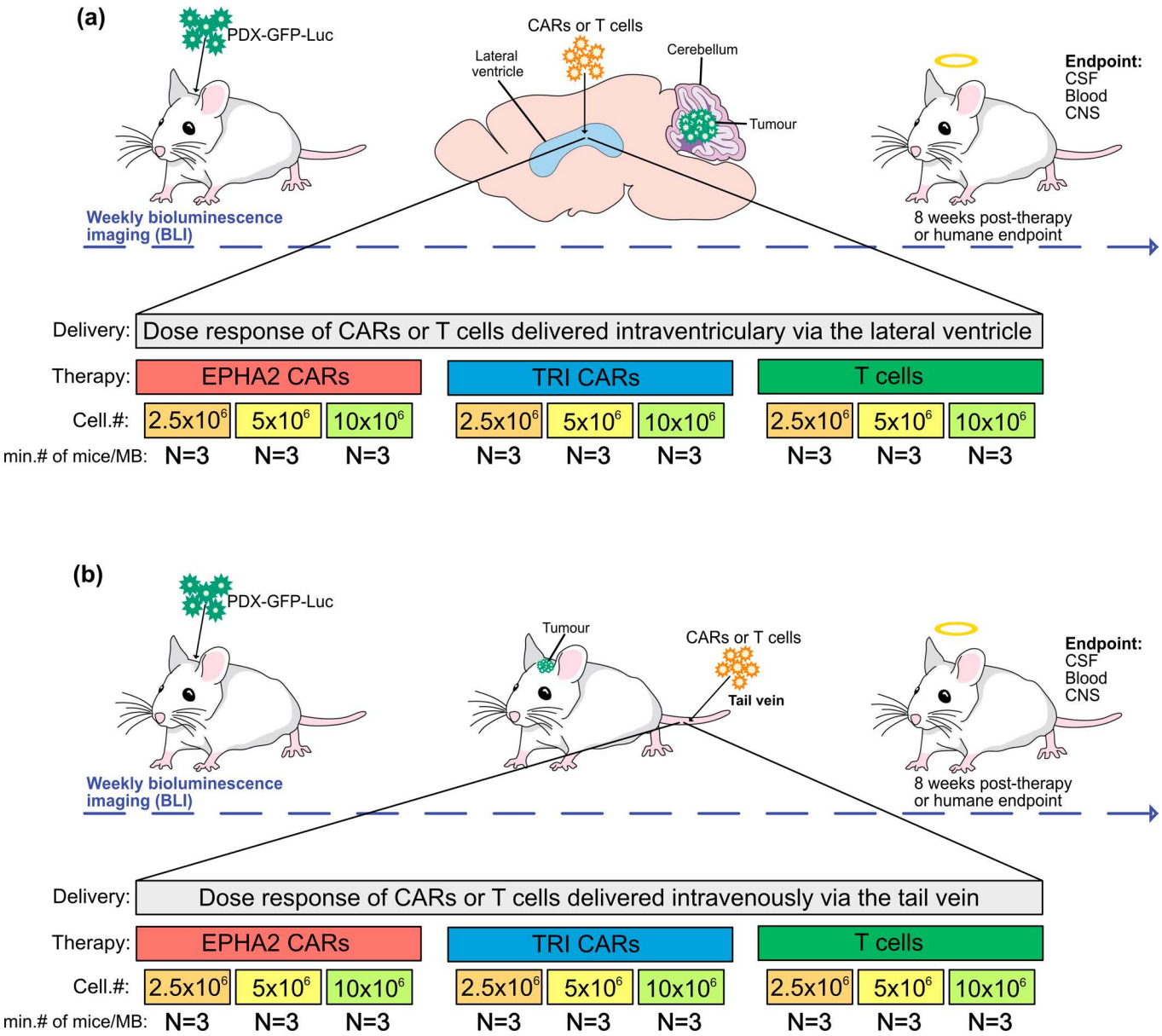

Extended Data Fig. 7 | *In vivo* potency trial, experimental scheme. Medulloblastoma cells (Med114FH or Med411FH) expressing eGFP-firefly luciferase (PDX-GFP-Luc) were xenografted into the cerebellum of NSG mice. BLI was performed to determine tumour engraftment, at which point a single dose of EPHA2 CAR T cells, TRI CAR T cells or non-transduced T cells, were delivered at dose range of 2.5×10^6, 5×10^6 or 10×10^6 **a**, intraventricularly by the lateral ventricle or **b**, IV by the tail vein. Tumour burden was monitored weekly by bioluminescence (BLI) until 8 weeks post-therapy, or humane endpoint. At endpoint, a terminal cardiac puncture was performed for complete blood collection, CSF removed from the cisterna magna, and CNS harvested.

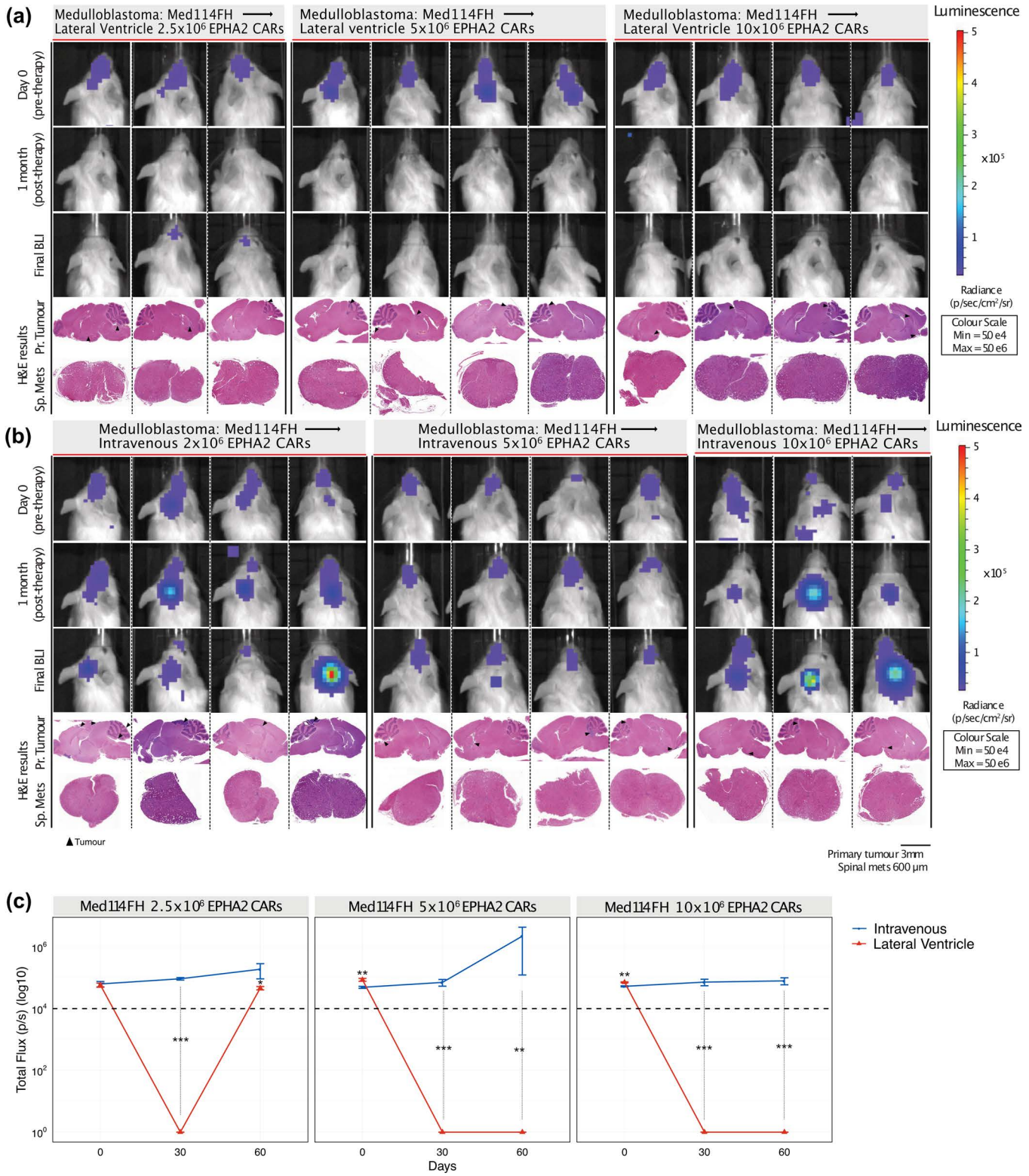

Extended Data Fig. 8 | *In vivo* potency trial endpoints of Med114FH PDXs treated with EPHA2 CAR T cells. Bioluminescence (BLI) and endpoint Hematoxylin-eosin (H&E) staining analysis of NSG mice xenografted with luciferase-expressing Med114FH, infused **a**, via the lateral ventricle or **b**, IV with EPHA2 CAR T cells at dose range of 2.5×10^6, 5.0×10^6 and 10×10^6 as indicated (colour map for all images indicates radiance, min = 5×10^4, max = 5×10^6). Each column represents one mouse, each row represents the indicated time point and subsequent final BLI. Results representative of 2 independent replicates. **c**, Measurement of tumour burden over time expressed as Total Flux (photons/s) following one round of lateral ventricle versus IV EPHA2 CAR T cell therapy. ***P < 0.0005, **P < 0.005, *P < 0.05, by two-sided ANOVA followed by Tukey post hoc test, n = 3 EPHA2 CAR T cells delivered intrathecally, n = 3 EPHA2 CARs T cells delivered IV for each dose range, centre lines show the mean ± SEM performed in triplicate. Infusion of 2.5×10^6 EPHA2: Day 0 IV vs LV P = 0.807, Day 30 IV vs LV P = 0.00009, Day 60 IV vs LV P = 0.07; 5.0×10^6 EPHA2: Day 0 IV vs LV P = 0.03, Day 30 IV vs LV P = 0.00007, Day 60 IV vs LV P = 0.001; 10×10^6 EPHA2: Day 0 IV vs LV P = 0.003, Day 30 IV vs LV P = 0.00007, Day 60 IV vs LV P = 0.000015.

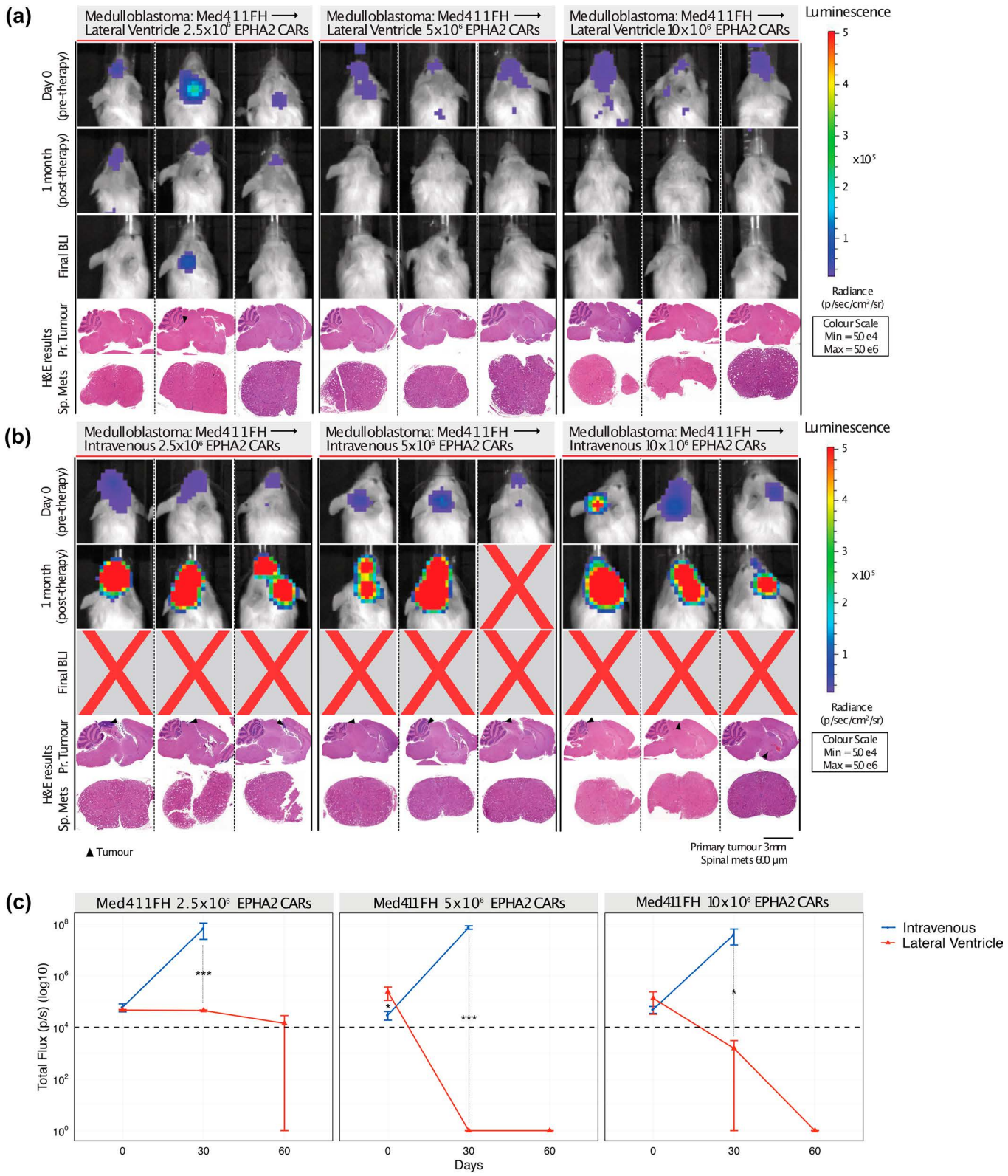

Extended Data Fig. 9 | *In vivo* potency trial endpoints of Med411FH PDXs treated with EPHA2 CAR T cells. Bioluminescence (BLI) and endpoint Hematoxylin-eosin (H&E) staining analysis of NSG mice xenografted with luciferase-expressing Med411FH, infused **a**, via the lateral ventricle or **b**, IV with EPHA2 CAR T cells at dose range of 2.5×10⁶, 5.0×10⁶ and 10×10⁶ as indicated (colour map for all images indicates radiance, min = 5×10⁴, max = 5×10⁶). Each column represents one mouse, each row represents the indicated time point and subsequent final BLI. Results representative of 2 independent replicates. **c**, Measurement of tumour burden over time expressed as Total Flux (photons/s) following one round of lateral ventricle versus IV EPHA2 CAR T cell therapy. ***P < 0.0005, **P < 0.005, *P < 0.05, by ANOVA followed by Tukey post hoc test, n = 3 EPHA2 CAR T cells delivered intrathecally, n = 3 EPHA2 CARs T cells delivered IV for each dose range, centre lines show the mean ± SEM performed in triplicate. Infusion of 2.5×10⁶ EPHA2: Day 0 IV vs LV P = 0.7, Day 30 IV vs LV P = 0.0004; 5.0×10⁶ EPHA2: Day 0 IV vs LV P = 0.03, Day 30 IV vs LV P = 0.00009; 10×10⁶ EPHA2: Day 0 IV vs LV P = 0.6, Day 30 IV vs LV P = 0.029.

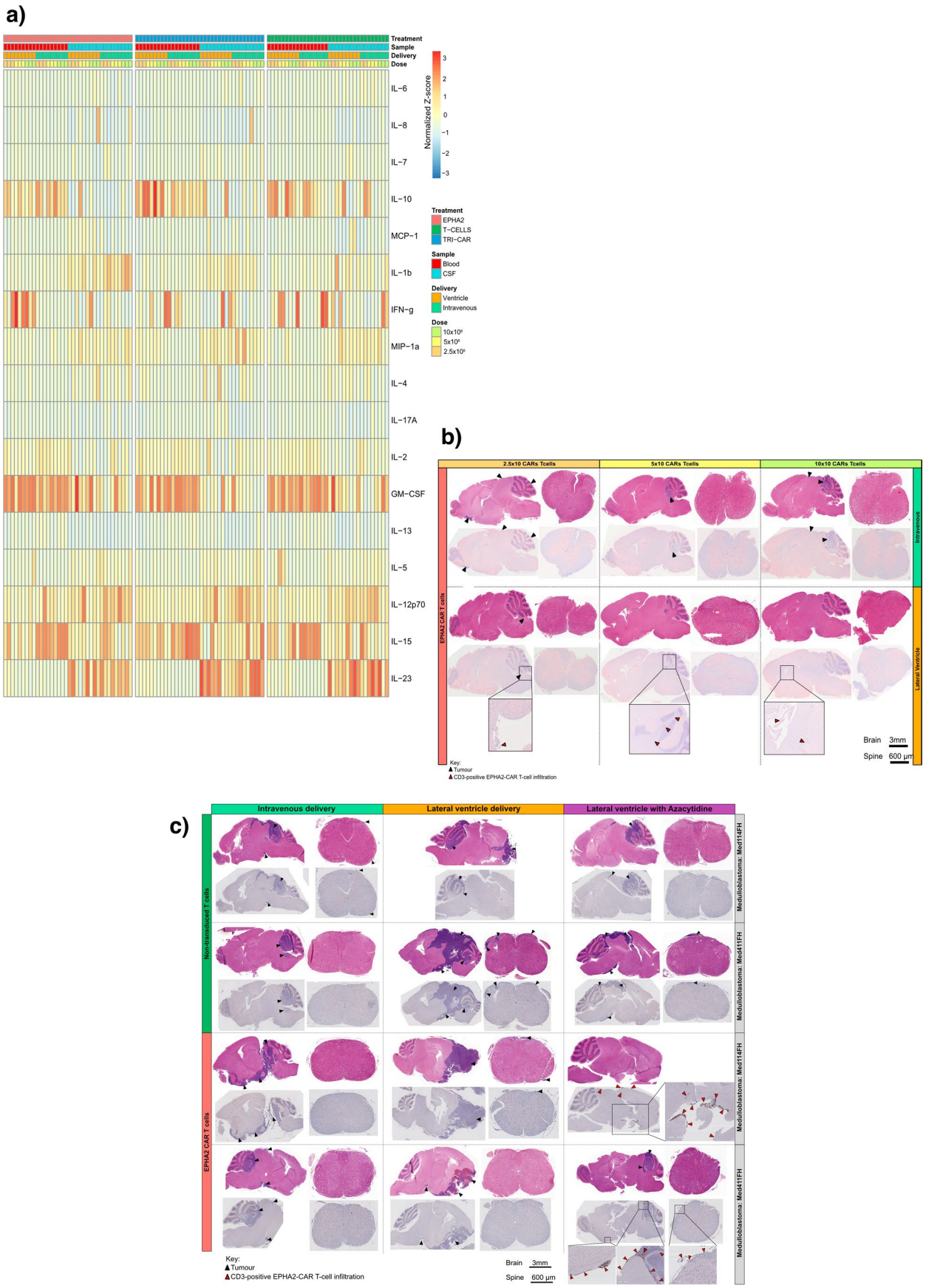

Extended Data Fig. 10 | See next page for caption.

Extended Data Fig. 10 | Activation of CAR T cells - *in vivo* potency trial. a, Heatmap of the normalized Z-scores of Human cytokines associated with T cell activation and augmentation, present in the blood circulation and CSF of NSG mice, in response to 2.5×10^6, 5.0×10^6 and 10×10^6 EPHA2 CAR T cells, TRI CAR T cells, or non-transduced T cells; delivered intraventricularly via the lateral ventricle, or IV via the tail vein. N = 36 EPHA2 (n = 16 blood and 16 CSF independent animal samples; n = 9 lateral ventricle and 9 intravenous CARs or T-cell infusions; n = 3 2.5×10^6, 3 5.0×10^6 and 3 10×10^6 CAR T-cell or non-transduced T-cell infusions., Samples were harvested 8 weeks post therapy, or at humane endpoint. **b**, IHC analysis of EPHA2 CAR T cell accumulation in mice treated within the associated *in vivo* potency trial, as indicated by CD3-positive protein expression. Top panel denotes mice infused IV with a dose range of 2.5×10^6, 5.0×10^6 and 10×10^6 EPHA2 CAR T cells, the bottom panel denotes mice infused intraventricularly via the lateral ventricle with a dose range of 2.5×10^6, 5.0×10^6 and 10×10^6 EPHA2 CAR T cells. Red arrows indicate EPHA2 T cell infiltration. Results representative of 2 independent replicates. **c**, IHC analysis of EPHA2 CAR T cell accumulation from archival FFPE samples of trial treated mice. The top panel denotes mice infused with non-transduced T cells, the bottom panel indicates mice treated with EPHA2 CAR T cells either intravenously (left), intraventricularly by the lateral ventricle (LV) (middle) or LV combined with Azacytidine (right) with a dose range of 5.0×10^6. Results representative of 2 independent replicates, red arrows indicate EPHA2 T cell infiltration.

nature research

Corresponding author(s): Michael D. Taylor

Last updated by author(s): Feb 19 2020

Reporting Summary

Nature Research wishes to improve the reproducibility of the work that we publish. This form provides structure for consistency and transparency in reporting. For further information on Nature Research policies, see Authors & Referees and the Editorial Policy Checklist.

Statistics

For all statistical analyses, confirm that the following items are present in the figure legend, table legend, main text, or Methods section.

n/a	Confirmed	
☐	☒	The exact sample size (*n*) for each experimental group/condition, given as a discrete number and unit of measurement
☐	☒	A statement on whether measurements were taken from distinct samples or whether the same sample was measured repeatedly
☐	☒	The statistical test(s) used AND whether they are one- or two-sided *Only common tests should be described solely by name; describe more complex techniques in the Methods section.*
☐	☒	A description of all covariates tested
☐	☒	A description of any assumptions or corrections, such as tests of normality and adjustment for multiple comparisons
☐	☒	A full description of the statistical parameters including central tendency (e.g. means) or other basic estimates (e.g. regression coefficient) AND variation (e.g. standard deviation) or associated estimates of uncertainty (e.g. confidence intervals)
☒	☐	For null hypothesis testing, the test statistic (e.g. *F*, *t*, *r*) with confidence intervals, effect sizes, degrees of freedom and *P* value noted *Give P values as exact values whenever suitable.*
☒	☐	For Bayesian analysis, information on the choice of priors and Markov chain Monte Carlo settings
☒	☐	For hierarchical and complex designs, identification of the appropriate level for tests and full reporting of outcomes
☒	☐	Estimates of effect sizes (e.g. Cohen's *d*, Pearson's *r*), indicating how they were calculated

Our web collection on statistics for biologists contains articles on many of the points above.

Software and code

Policy information about availability of computer code

Data collection	The datasets analysed during the current study are open source, referenced and available from the following repositories: primary-metastasis medulloblastoma pairs DNA methylation analysis GSE63670; primary medulloblastoma genome-wide methylation and expression profile analysis GSE85218; primary ependymoma Affymetrix chip array analysis GSE27279. Flow cytometry data collection was performed using a BD Biosciences LSRII CFI VBYR. Bioluminescence imaging data collection was performed using an Xenogen Spectrum (IVIS-200) imaging system.
Data analysis	All software used in this study for data analysis are either commercially available or open source and referenced were applicable. No custom codes were used for data analysis. Flow cytometry analysis was performed using FlowJo version 10.0.7. Bioluminescence imaging analysis was performed using Living Image Software (PerkinElmer) version 4.0.

For manuscripts utilizing custom algorithms or software that are central to the research but not yet described in published literature, software must be made available to editors/reviewers. We strongly encourage code deposition in a community repository (e.g. GitHub). See the Nature Research guidelines for submitting code & software for further information.

Data

Policy information about availability of data

All manuscripts must include a data availability statement. This statement should provide the following information, where applicable:

- Accession codes, unique identifiers, or web links for publicly available datasets
- A list of figures that have associated raw data
- A description of any restrictions on data availability

The datasets analysed during the current study are open source, referenced and available from the following repositories: primary-metastasis medulloblastoma pairs DNA methylation analysis GSE63670; primary medulloblastoma genome-wide methylation and expression profile analysis GSE85218; primary ependymoma Affymetrix chip array analysis GSE27279.

Field-specific reporting

Please select the one below that is the best fit for your research. If you are not sure, read the appropriate sections before making your selection.

☒ Life sciences ☐ Behavioural & social sciences ☐ Ecological, evolutionary & environmental sciences

For a reference copy of the document with all sections, see nature.com/documents/nr-reporting-summary-flat.pdf

Life sciences study design

All studies must disclose on these points even when the disclosure is negative.

Sample size	As the same experimental conditions, variances, and co-variances will be used, the use of a MANOVA with A Priori power analysis was employed to determine initial in vivo trial sample sizes. For in vitro studies, n=3 or n=4 biologically independent replicates derived from different wells per group were used. This sample size is often reported in previous publications to be sufficient for a confident data analysis and we found this sample size is sufficient to control for technical variations.
Data exclusions	No data was excluded from this study
Replication	We confirmed all attempt to replicate experiments were successful. Immunohistochemistry analysis was performed in at least duplicate verifying the initial protein expression observed, all appropriate optimizations and controls were employed. Replications for medulloblastoma PDXs Med114FH, Med411FH and MMB-MDT using a single intraventricular and single intravenous, repeat dose intraventricular, and combined azacytidine intraventricular infusion of associated CAR-T-cells or non-transduced T-cell controls were performed in a minimum of n=3 to validate the treatment results. All replications were successful.
Randomization	In the murine experiments, mice were injected with medulloblastoma or ependymoma and randomly distributed (without bias from the luciferase imaging of tumour burden) to experimental groups. For the in vitro experiments, multiple cell cultures were grown and randomly assigned for ELISA or flow cytometry analysis.
Blinding	In the murine experiments, mice were randomly distributed to experimental groups immediately following tumour engraftment, without bias from luciferase imaging of tumour burden. Clinical endpoints were assessed and assigned by veterinary technicians blinded to tumour type and experimental group. All in vitro experiments were processed in a blindly.

Reporting for specific materials, systems and methods

We require information from authors about some types of materials, experimental systems and methods used in many studies. Here, indicate whether each material, system or method listed is relevant to your study. If you are not sure if a list item applies to your research, read the appropriate section before selecting a response.

Materials & experimental systems

n/a	Involved in the study
☐	☒ Antibodies
☐	☒ Eukaryotic cell lines
☐	☐ Palaeontology
☐	☒ Animals and other organisms
☐	☐ Human research participants
☐	☐ Clinical data

Methods

n/a	Involved in the study
☐	☐ ChIP-seq
☐	☒ Flow cytometry
☐	☐ MRI-based neuroimaging

Antibodies

Antibodies used	IL13RA2 (Abcam lot:GR270853 1:200), HER2/CB11 (BioGenex MU134C, lot:MU1340517 1:400) and EPHA2 (Abnova MAB1769, lot:A091240 1:500) IL13Ra2 (R&D Systems AF146, 1:400, lot:CZT091806A), HER2 (Sigma HPA001383, 1:500, lot:B116400), EPHA2 (Abcam ab150304, 1:75ss, lot:GR3206483-2) IL13Ra2 (Abcam, ab55275, lot:GR2945771, 1 µg/µl, 1:100), Anti-HER-2/neu (Becton Dickinson, 340554, lot:7333811, 1:50), EPHA2 (R&D Systems, MAB3035, 0.25 µg/µl, 1:4, lot:3184103-1). CD3 (Abcam ab16669, lot:GR3307114-1, 1:100) PI (1:1000, Invitrogen, F1930, lot:7333811) Sytox Blue (1:1000, ThermoFisher, S34857, lot:unavailable) Dapi (1:1000, Roche, 10236276001, lot:15733122)
Validation	All antibodies used were initially validated by the suppliers.

All antibodies used in this study have been tested by the manufacture and have been cited by other authors and references are available on the websites of the manufacture. Appropriate controls positive negative controls, as defined by each antibody supplier, and as defined in the manuscript, were used.

Eukaryotic cell lines

Policy information about cell lines

Cell line source(s)	Med114FH and Med411FH purchased from the Brain Tumour Resource Lab (Fred Hutchinson Cancer Research Centre). MDT-MMB, MDT-PFA4 and MDT-PFA5 - derived at in the Taylor Lab, The Hospital for Sick Children. PFA-Ep612 was a gift from Stephen Keir, Duke Cancer Institute. (HEK) 293T-cells were purchased from the ATCC (ATCC® CRL-3216™).
Authentication	All lines authenticated with STR profiling.
Mycoplasma contamination	All cells tested negative for mycoplasma.
Commonly misidentified lines (See ICLAC register)	No commonly mis-identified cell lines were used

Palaeontology

Specimen provenance	n/a
Specimen deposition	n/a
Dating methods	n/a

☐ Tick this box to confirm that the raw and calibrated dates are available in the paper or in Supplementary Information.

Animals and other organisms

Policy information about studies involving animals; ARRIVE guidelines recommended for reporting animal research

Laboratory animals	Between 6 - 10 week old Male and female Non-Obese Diabetic, SCID, gamma KO (NSG) mice were use for xenograft studies.
Wild animals	The study did not involve wild animals.
Field-collected samples	The study did not involve field-collected samples.
Ethics oversight	The Animal Use Protocol was reviewed and approved annually by the Animal Care Committee at The Centre for Phenogenomics in Toronto

Note that full information on the approval of the study protocol must also be provided in the manuscript.

Human research participants

Policy information about studies involving human research participants

Population characteristics	All human tumour samples were used in accordance with the Research Ethics Board at the Hospital for Sick Children (Toronto, Canada), protocol REB1000024587. The donor peripheral blood mononuclear cells (PBMCs) were derived using the Institutional Review Board approved protocol H-15280 at Baylor College of Medicine, Texas, United States.
Recruitment	n/a
Ethics oversight	All human tumour samples were used in accordance with the Research Ethics Board at the Hospital for Sick Children (Toronto, Canada), protocol REB1000024587. The donor peripheral blood mononuclear cells (PBMCs) were derived using the Institutional Review Board approved protocol H-15280 at Baylor College of Medicine, Texas, United States.

Note that full information on the approval of the study protocol must also be provided in the manuscript.

Clinical data

Policy information about clinical studies

All manuscripts should comply with the ICMJE guidelines for publication of clinical research and a completed CONSORT checklist must be included with all submissions.

Clinical trial registration	n/a
Study protocol	n/a
Data collection	n/a
Outcomes	n/a

ChIP-seq

Data deposition

☐ Confirm that both raw and final processed data have been deposited in a public database such as GEO.

☐ Confirm that you have deposited or provided access to graph files (e.g. BED files) for the called peaks.

Data access links *May remain private before publication.*	n/a
Files in database submission	n/a
Genome browser session (e.g. UCSC)	n/a

Methodology

Replicates	n/a
Sequencing depth	n/a
Antibodies	n/a
Peak calling parameters	n/a
Data quality	n/a
Software	n/a

Flow Cytometry

Plots

Confirm that:

☐ The axis labels state the marker and fluorochrome used (e.g. CD4-FITC).

☐ The axis scales are clearly visible. Include numbers along axes only for bottom left plot of group (a 'group' is an analysis of identical markers).

☐ All plots are contour plots with outliers or pseudocolor plots.

☒ A numerical value for number of cells or percentage (with statistics) is provided.

Methodology

Sample preparation	Required information detailed in 'Flow cytometry and sample preparation' methods section.
Instrument	Becton Dickinson (BD) analyzer, LSRII-CFI, VBGR
Software	FlowJo used for analysis of samples
Cell population abundance	n/a
Gating strategy	Appropriate sample controls used to ensure optimal gating strategies for assessment of cell samples via flow cytometry: negative for primary antibody, viability-gating, and unstained controls; information detailed in 'Flow cytometry and sample preparation'.

☐ Tick this box to confirm that a figure exemplifying the gating strategy is provided in the Supplementary Information.

Magnetic resonance imaging

Experimental design

Design type	n/a
Design specifications	n/a
Behavioral performance measures	n/a

Acquisition

Imaging type(s)	n/a
Field strength	n/a
Sequence & imaging parameters	n/a
Area of acquisition	n/a

Diffusion MRI ☐ Used ☐ Not used

Preprocessing

Preprocessing software	n/a
Normalization	n/a
Normalization template	n/a
Noise and artifact removal	n/a
Volume censoring	n/a

Statistical modeling & inference

Model type and settings	n/a
Effect(s) tested	n/a

Specify type of analysis: ☐ Whole brain ☐ ROI-based ☐ Both

Statistic type for inference (See Eklund et al. 2016)	n/a
Correction	n/a

Models & analysis

n/a	Involved in the study
☒	☐ Functional and/or effective connectivity
☒	☐ Graph analysis
☒	☐ Multivariate modeling or predictive analysis